A recurrent mutation in *CACNA1G* alters Cav3.1 T-type calcium channel conduction and causes autosomal dominant cerebellar ataxia

Marie Coutelier,[1,2,3,4,5,6,19] Iulia Blesneac,[7,8,19] Arnaud Monteil,[7,8] Marie-Lorraine Monin,[1,2,3,4,9] Kunie Ando,[1,2,3,4,10] Emeline Mundwiller,[4] Alfredo Brusco,[11,12] Isabelle Le Ber,[1,2,3,4,13] Mathieu Anheim,[14,15,16] Anna Castrioto,[17,18] Charles Duyckaerts,[1,2,3,4,10] Alexis Brice,[1,2,3,4,9] Alexandra Durr,[1,2,3,4,9] Philippe Lory,[7,8,20] Giovanni Stevanin[1,2,3,4,6,9,20*]

[1] INSERM, U 1127, F-75013, Paris, France; [2] CNRS, UMR 7225, F-75013, Paris, France; [3] Sorbonne Universités, UPMC Univ Paris 06, UMRS_1127, F-75013, Paris, France; [4] Institut du Cerveau et de la Moelle épinière, ICM, F-75013, Paris, France; [5] Laboratory of Human Molecular Genetics, de Duve Institute, Université catholique de Louvain, B-1200, Brussels, Belgium; [6] Ecole Pratique des Hautes Etudes, F-75014, Paris, France; [7] Institut de Génomique Fonctionnelle, CNRS UMR 5203, INSERM, U 1191, Université de Montpellier, F-34094, Montpellier, France; [8] LabEx 'Ion Channel Science and Therapeutics', F-34094, Montpellier, France; [9] APHP, Centre de référence de Neurogénétique, Hôpital de la Pitié-Salpêtrière, F-75013, Paris, France; [10] Laboratoire de Neuropathologie Escourolle, Hôpital de la Pitié-Salpêtrière, F-75013, Paris, France; [11] Department of Medical Sciences, University of Turin, 10126, Turin, Italy; [12] Medical Genetics Unit, Città della Salute e della Scienza University Hospital, 10126, Turin, Italy; [13] AP-HP, Hôpital de la Pitié-Salpêtrière, Fédération des maladies du système nerveux, F-75013, Paris, France; [14] Département de Neurologie, Hôpital de Hautepierre, CHU de Strasbourg, F-67098, Strasbourg, France; [15] Institut de Génétique et de Biologie Moléculaire et Cellulaire (IGBMC), INSERM-U964/CNRS-UMR7104/Université de Strasbourg, F-67400, Illkirch, France; [16] Fédération de Médecine Translationnelle de Strasbourg (FMTS), Université de Strasbourg, F-67081, Strasbourg, France; [17] Pole de Neurologie et Psychiatrie, Unité troubles du Mouvement, CHU de Grenoble, F-38700, Grenoble, France; [18] Equipe Fonctions cérébrales et Neuromodulation, Grenoble Institut des Neurosciences, INSERM U836-UJF-CEA-CHU, F-38700, Grenoble, France

[19] These authors contributed equally to this work

[20] These authors contributed equally to this work

* Correspondence: giovanni.stevanin@upmc.fr

Summary

Hereditary cerebellar ataxias (CA) are neurodegenerative disorders, clinically characterized by a cerebellar syndrome, often accompanied by other neurological or non-neurological signs. All transmission modes have been described. In autosomal dominant forms (ADCA), mutations in more than 30 genes are implicated, but the molecular diagnosis remains unknown in about 40% of the cases. Implication of ion channels has long been an on-going topic in the genetics of CA, and mutations in several channel genes have been recently connected to ADCA.

In a large family with ADCA and mild pyramidal signs, we searched for the causative variant with a combined approach of linkage analysis and whole exome sequencing. We identified a NM_018896.4:c.5144G>A mutation in *CACNA1G*, causing an arginine-to-histidine (p.Arg1715His) change in the voltage-sensor/segment S4 of the T-type Cav3.1 channel protein. Two out of 479 index cases screened subsequently harbored the same mutation. Electrophysiological experiments were performed in HEK293T cells to compare the properties of the p.Arg1715His and the wild-type Cav3.1 channels. The current-voltage and the steady-state activation curves of the p.Arg1715His channel were shifted positively, while the inactivation curve had a higher slope factor. Computer modelisation in deep cerebellar nuclei neurons suggested that the mutation results in decreased neuronal excitability.

Taken together, these data establish *CACNA1G*, which is highly expressed in the cerebellum, as a gene whose mutations can cause ADCA. This is consistent with the neuropathological examination showing severe Purkinje cell loss. Our study further extends our knowledge of the link between calcium channelopathies and CA.

Hereditary cerebellar ataxias are rare clinically and genetically heterogeneous neurodegenerative disorders.[1] They are characterized by a cerebellar syndrome, associated with other neurological or extra-neurological symptoms, and are inherited in all classical transmission modes. In autosomal dominant cerebellar ataxias (ADCA), the most frequent mutations are trinucleotide CAG repeat expansions, present in seven genes[2], coding for a polyglutamine stretch in the corresponding proteins. Next mutations in frequency are noncoding nucleotide expansions and conventional mutations that have been described in more than 20 different genes. The causative variant remains unknown, however, in about 40% of individuals with ADCA.[2; 3]

Over the last few years, next generation sequencing has led to the identification of an increasing number of variants in many genes implicated in this pathology.[4] Mutations in multiple genes gathered in various common pathways have highlighted their importance in the physiopathology of ADCAs, including channels. The first channel-coding gene to be involved in ADCAs was *CACNA1A* (MIM *601011), encoding the P/Q-type voltage-gated calcium channel; small polyglutamine expansions, loss-of-function mutations, or missense variants in this gene give rise to Spinocerebellar Ataxia type 6 (MIM #183086), Episodic Ataxia type 2 (MIM #108500), or Familial Hemiplegic Migraine type 1 (MIM #141500).[5; 6] Knockdown of the fibroblast growth factor gene, *FGF14* (MIM *601515), responsible for SCA27 (MIM #609307), reduces calcium currents in granule cells.[7] Mutations in other ion channel genes have also been described, including the voltage-gated potassium channel genes *KCNC3*/SCA13 (MIM *176264/#605259)[8] and *KCND3*/SCA19-22 (MIM *605411/#607346),[9; 10] and the ligand-gated ion channel genes *ITPR1*/SCA15 (MIM *147265/#606658) and *GRID2* (MIM *602368).[1; 11; 12] All these findings converge to emphasize the importance of ion balance, notably that of calcium ions, in cerebellar physiology.[13]

In this paper, we report three pedigrees segregating ADCA, with a recurrent mutation inducing an amino acid change in the voltage sensor S4 segment of domain IV in Cav3.1, a T-type calcium channel encoded by *CACNA1G* (MIM *604065). We present electrophysiological *in vitro* evidence that this p.Arg1715His (NM_018896.4) variant alters the channel activity, shifting its steady-state activation curve towards more positive values and changing its inactivation slope constant. In an *in silico* model

of deep cerebellar nuclei neurons, we establish decreased excitability linked to these altered parameters. Altogether, we describe a monogenic disease linked to *CACNA1G* mutations; confirm the implication of Cav3.1 channels, highly expressed in Purkinje cells and deep cerebellar nuclei neurons, in cerebellar physiology; and strengthen the gathering of evidence towards the prominence of calcium levels in cerebellar ataxia pathophysiology.

Families AAD-SAL-233, AAD-GRE-319, and AAD-SAL-454 were part of the Spastic Paraplegia and ATAXia (SPATAX) network cohort, along with more than 500 other ADCA pedigrees. Affected members and relatives were examined and blood was taken after informed consent, according to French legislation (Paris Necker ethics committee approval to A. Brice and A. Durr, RBM 01-29 and RBM 03-48). All clinical data are summarized in Table 1. The age at onset varied widely, ranging from 9 to 78 years; gait instability was the major presenting symptom (9/10). Even after decades of progression, the disability and symptoms remained mild to moderate, indicating stable cerebellar involvement. Ocular signs, including saccadic pursuit, horizontal nystagmus and transient diplopia, were often noted (7/10). Interestingly, pyramidal signs, ranging from reflex pyramidal syndrome to spastic gait, were present in 5/10 individuals. Of note, depression was reported in 3/10 individuals, and cognitive impairment in 2/10. When performed (n=5), MRI revealed predominantly vermian cerebellar atrophy and a normal pons (Figure S1).

Individual AAD-SAL-233-14 (III-9 in Figure 2) had signed an informed consent for brain donation. She died at age 83. The left hemi-brain was examined, while samples from the right hemi-brain were frozen and kept in the brain bank GIE NeuroCEB (Bioresource Research Impact Factor number = BRIF BB-0033-00011), declared to the Ministry of Research and Higher Education as required by the French law. The Brain Bank has been officially authorized to provide samples to scientists (agreement AC-2007-5). Macroscopically, the cerebellar hemisphere and the vermis were respectively mildly and severely atrophic. The cerebral cortex appeared normal. Microscopically, the volume of the cerebellar white matter was reduced. Bergmann gliosis and empty baskets were evidences of loss of Purkinje cells, more prominent in the vermis. In the granular layer, the number of glomeruli was decreased. The cellular density was increased in the molecular layer, which appeared loosened (Figure 1).

Unusually abundant polyglycosan bodies were observed in all cerebellum layers. The neuronal density in the dentate nucleus was normal as was the density of myelinated axons in the hilus. There was no neuronal loss in the pontine nuclei. The number of neurons was reduced in the inferior olive, which appeared gliotic. The substantia nigra was normal.

Microscopic evidences of Alzheimer's disease (MIM #104300) were also observed, with amyloid deposits in the cerebral cortex, the hippocampus and the basal ganglia (Thal phase 3 [14]). Tau positive neurofibrillary tangles, neuropil threads and senile plaques coronae were seen in the entorhinal cortex and hippocampus. Associative cortices were mildly affected and primary cortices, spared (Braak stage V [15]).

Polyglutamine and *C9orf72* (MIM *614260) expansions had previously been excluded in all three index cases using classical procedures. Linkage analysis was performed in family AAD-SAL-233 (Figure S2). Six major putative loci were detected, with maximal multipoint LOD scores ranging from +1.579 to +2.279. Whole exome sequencing was performed in individuals AAD-SAL-233-15 (III-10 in Figure 2) and AAD-SAL-233-25 (IV-16 in Figure 2), with 85 to 87% 30x-coverage, through enrichment capture using the Sure Select All Exon 50Mb kit (Agilent) followed by 2x75bp massive parallel sequencing in the Hiseq2000 sequencer (Illumina) (Table S1). Results were analyzed using the following criteria: effect on the coding sequence of an established protein-coding gene, heterozygous state in affected individual 25 and absent from healthy individual 15, location within the non-excluded loci, frequency under 0.1% in public databases (dbSNP137, Exome Variant Server, EXome Aggregation Consortium). Sanger validation and segregation study in all family members led to the identification of two candidate variants: a chr10:g.95372766G>A, NM_006204.3: c.284G>A: p.Arg95His change in *PDE6C* (MIM *600827) and a chr17: g.48694921G>A, NM_018896.4: c.5144G>A: p.Arg1715His change in *CACNA1G* (MIM *604065) (Figure 2, Table S2). Of note, *PDE6C* is much more tolerant to missense variations than *CACNA1G*, as estimated by Samocha et al.,[16] with an observed to expected ratio of 236/261.5 (Z-score 0.77), compared to 598/903.6 (Z-score 4.97) for *CACNA1G*.

We then screened ADCA index cases for variants in *CACNA1G* (n=479), *PDE6C* and genes previously involved in ADCA (n=384), with amplicon-based panel sequencing techniques, either with conventional PCR amplification followed by GS Junior (Roche) sequencing (n=95) or microfluidic PCR amplification (Fluidigm Access Array) followed by MiSeq (Illumina) sequencing (n=384) according to the manufacturers protocols (Table S3). Results were analyzed using the above-mentioned criteria. Two index cases, AAD-GRE-319-12 (II-2 in Figure 2), and AAD-SAL-454-10 (III-1 in Figure 2), harbored the same *CACNA1G* NM_018896.4: c.5144G>A: p.Arg1715His variant. No recurrence of the abovementioned *PDE6C* variant was observed. All detected *PDE6C* variants, reported in Table S4, were present in public databases.

No conventional mutations in genes previously involved in ADCA were found in AAD-GRE-319-12 (II-2 in Figure 2). AAD-SAL-454-10 (III-1 in Figure 2) also harbored a Variant of Unknown Significance (class 3 ACMG) in *SPTBN2*/SCA5 (MIM *604985/#600224), chr11: 66455764, NM_006946.2: c.6250G>A: p.Glu2084Lys, not located within the spectrin repeats as previously described for all *SPTBN2* mutations.[17] It was reported at the heterozygous state in one individual in EVS and one other case in ExAC; almost all *in silico* prediction softwares matched to predict it to be tolerated (data not shown). No recurrence was observed in the other 383 index cases tested.

Segregation of the *CACNA1G* c.5144G>A (p.Arg1715His) variant was established in two additional affected members of family AAD-GRE-319 (Figure 2). Other individuals harbored various *CACNA1G* variants (Table S5); however, their pathogenic effects could not be ascertained, due to the lack of affected individuals for segregation studies, genetic elements suggesting deleterious effects, or electrophysiological anomalies (Table S6). Analysis of flanking variants identified two homozygous variants in the *CACNA1G* region (chr17:g.48652875A>G and chr17:g.48655493A>G) in individual AAD-SAL-454-10 (III-1 in Figure 2) that were absent in AAD-SAL-233-25 (IV-16 in Figure 2) and heterozygous in AAD-GRE-319-12 (II-2 in Figure 2), excluding a common founder effect for all three families.

We hence focused on the *CACNA1G* variant versus the *PDE6C* one, because of strict co-segregation with the disease, absence in public databases, more concordant pathogenicity prediction scores, slightly higher conservation scores (Table S2), lower tolerance to missense variation, extremely high expression in the cerebellum,[18-20] and

the previous implication of *CACNA1A* as well as other ion channels in cerebellar ataxias.

To study the effect of the p.Arg1715His variant on the electrophysiological characteristics of Cav3.1, the c.5144G>A mutation was introduced into the cDNA of the human Cav3.1 channel (isoform 5, Uniprot O43497-1, [21]) by site directed mutagenesis (QuickChange Lightning Site-Directed mutagenesis, Agilent technologies). The wild-type (WT) and mutant cDNA constructs were then transfected into HEK239T cells and macroscopic currents were recorded by whole-cell patch clamp techniques. Figure 3A shows typical recordings of the calcium current generated by these channels. Several differences between the WT and the p.Arg1715His channel were observed. Notably, the aberrant channel exhibited a significant shift of the steady-state activation curve towards more positive membrane potential values. The half-activation potential changed from -47.20 ± 0.65 mV (n=18) for the WT to -43.27 ± 0.73 mV (n=16) ($p<0.001$) (Figure 3B). The steady-state inactivation curve was also affected. Although the half-inactivation potential was unchanged (-70.91 ± 0.48 mV [n=15] for the WT vs 70.68 ± 0.36 mV [n=16] for p.Arg1715His), the slope factor was significantly higher for the aberrant channel (5.39 ± 0.11 mV (n=16) compared to 4.29 ± 0.07 mV (n=15) for the WT, $p<0.0001$). As a consequence, the window current also shifted towards more positive membrane potentials (Figure 3D). No significant change was observed in current density or other biophysical properties of the channel, such as activation and inactivation kinetics (Figure 3E-F), recovery from inactivation (Figure 3G) or deactivation kinetics (Figure 3H). T-type calcium channels, especially Cav3.1, are highly expressed in cerebellar neurons, including deep cerebellar nuclear (DCN) neurons[22]. To determine the functional consequences that the p.Arg1715His change could have on firing, we used a DCN computer model[23], with both excitatory and inhibitory inputs from 150 mossy fibers and 450 Purkinje cell synapses respectively. Introduction of our experimental parameters for the steady state activation and inactivation curves in this model revealed alteration of DCN firing properties. Notably, the p.Arg1715His change led to a diminution of the number of spikes per burst (4 spikes compared to 5 for the WT, Figure 3I) and a delayed onset of burst firing, thus increasing the interval between the bursts (Figure 3I). These results suggest that the p.Arg1715His channel is responsible for a decrease in the neuronal excitability.

The Cav3.1 channel belongs to the family of voltage-gated calcium channels (VGCCs), a large family divided in two main subgroups: (i) low-voltage activated (LVA) VGCCs, also known as T-type, comprising the Cav3.1 encoded by *CACNA1G*, Cav3.2, and Cav3.3 isoforms; and (ii) high-voltage activated (HVA) VGCCs, further divided into L-type, P/Q-type, N-type and R-type depending on their sensitivity to pharmacological agents.[24-26] VGCCs are major actors regulating the calcium entry into neurons, and in turn play predominant roles in membrane potential regulation, and also in the modulation of calcium signaling pathways, such as neurite outgrowth,[27] calcium-dependent gene transcription, neurotransmitter release, or regulation of enzymes such as protein kinase C,[26] whose gamma subunit is associated with Spinocerebellar Ataxia 14 (MIM #605361) when mutations occur in *PRKCG* (MIM *176980).[28] The variety of coexisting subtypes and isoforms allows the establishment of highly specific neuronal firing patterns.[26; 29; 30]

T-type Cav3 calcium channels differ from HVA-VGCCs by their ability to be activated and inactivated at low voltages, near the resting membrane potential, their faster recovery from inactivation, their slower deactivation, and a characteristic window current occurring in the range of the resting membrane potential of neurons.[31; 32] In this respect, they act as pacemakers and excitability regulators,[26] allowing cells to be depolarized at needed membrane potential for other channels' activation. This window current is also essential for the regulation of the intracellular calcium concentration.[33] In neurons, they have two essential behaviors: triggering of a burst action potential following a low threshold calcium spike[25; 32] and rebound burst firing.[26; 31; 32] Of the three Cav3 isoforms, Cav3.1 is highly expressed in cerebellar neurons, as well as thalamic relay neurons,[18; 20] where it plays a major role in the establishment of the slow (<1Hz) sleep oscillations of non-rapid eye movement sleep (REM).[31] Gain-of-function variants are thought to participate in the spike-and-wave discharges of thalamocortical neurons in absence epilepsy through enhancement of thalamic oscillatory activities.[18; 25; 34; 35]

In the cerebellum, a comprehensive study of Cav3 isoforms expression in neurons revealed that their specific patterns are correlated to various electrophysiological phenotypes.[30] *In situ* hybridization studies described *CACNA1G* mRNA in both Purkinje cells (PC) and deep cerebellar nuclei neurons (DCN).[20; 36] In

DCN, Cav3.1 is predominantly expressed in a subset of large neurons exhibiting a strong ability to generate rebound burst firing after hyperpolarization.[30; 37] Pharmacological evidences confirmed that these rebound bursts are mediated by T-type calcium channels.[38] They appear to be physiologically relevant and consistent with a response to inhibitory input from PCs.[39] Their characteristics result from interplay between T-type channels and hyperpolarization-activated cyclic-nucleotide channels (HCN).[22; 39] In PC, all three subtypes of Cav3 are expressed.[30] Cav3.1 was found at the cell body as well as at the synapse between parallel fibers (PF) and PC[19]. At this synapse, Cav3 channels interact with intermediate conductance calcium-activated potassium channels (IKCa) to suppress the temporal summation of background excitatory postsynaptic potentials from PF through an after hyperpolarization.[22; 40] This is essential to allow the detection of sensory-relevant high frequency inputs.[22; 40] Finally, PC burst firing was shown to rely on P/Q-type calcium current. In addition, T-type channels interact with large conductance calcium-activated potassium channels (BK) to determine firing rate, burst duration and interburst interval.[41] Therefore, T-type channels, Cav3 isoforms, and, more specifically, the Cav3.1 isoform, have major roles in the PF-PC-DCN signal processing. Of note, histologically, the neuronal density appeared normal in the dentate nucleus of our affected case; marked PC loss was observed.

In mice, that show 93% Cav3.1 amino-acid sequence identity with humans, no spontaneous *Cacna1g* mutations have been reported; however, several models have been generated. *Cacna1g* null mice have no overt neurological phenotype, normal growth and normal brain pathology;[42] in particular, they have no motor defects.[43] However, they present with a non-REM sleep disturbance,[44] are resistant to pharmacologically induced absence seizures,[42] show attenuated neuropathic pain,[45] and present bradycardia and slowed atrioventricular conduction.[46] The only cerebellar anomaly linked to *Cacna1g* inactivation was a loss of Purkinje cells in double mutant mice lacking both Cav3.1 and the *alpha*1 GABA-A receptor.[43] In this mouse model, motor defects, including tremor, were exacerbated compared to mice lacking only the GABA-A receptor. Conversely, transgenic mice overexpressing Cav3.1 show spontaneous spike-and-wave discharges associated with behavioral arrest.[18]

In human pathology, the role of T-type VGCCs has only been partially elucidated. In particular, no monogenic disease has clearly been linked to T-type channel gene mutations until now.[25; 47] *CACNA1H* (MIM *607904)/Cav3.2 is implicated in absence epilepsy (MIM #611942),[48-50] with several mutations leading to increased activity of the channel[51]. However, in many cases, the variant rather induces susceptibility to seizures rather than has a monogenic causative effect.[25; 49] As for *CACNA1G*, some variants have been described in Idiopathic Generalized Epilepsy (MIM %600669);[52] many if not all of them appear to be risk factor variants and not causative mutations. *CACNA1G* was also associated with autism spectrum disorder (MIM %209850), but the association was too weak to fully explain the odds ratio.[53] Finally, a large study on intellectual disability identified a homozygous *CACNA1G* frameshift variant in three siblings with associated cataracts, but no reported cerebellar ataxia.[54]

Despite its predominant expression in PC and DCN neurons, *CACNA1G* was never implicated by itself in cerebellar dysfunction. In three independent ADCA families, we describe the recurrent p.Arg1715His variant in Cav3.1. There are strong genetic arguments in favor of the deleteriousness of this variant: 1/ concordance of all *in silico* pathogenicity predictions; 2/ absence in all examined public databases (more than 60k exomes); 3/ amino acid conservation in all orthologs, paralogs, and S4 segments of all four domains of the protein; 4/ location within a putatively linked locus (Figure S2); 5/ absence of pathogenic variants in all genes previously involved in ADCA; 6/ recurrence of the mutation in three pedigrees with exclusion of a common founder effect; 7/ perfect segregation in both pedigrees where it could be verified; and 8/ location within a functionally important domain of the protein, the voltage sensor S4 segment. Importantly, in vitro studies showed that the variant altered electrophysiological characteristics of the channel, with activation at more positive voltages, an increased slope factor of the steady-state inactivation curve and, consequently, a shift of the window current towards more positive potentials. Minimal alterations in T-type VGCC properties can lead to marked alterations in firing dynamics.[55] Simulation of a DCN neuron activity carrying either WT or p.Arg1715His Cav3.1 parameters also revealed a difference in burst firing, suggesting a reduced neuronal excitability caused by the aberrant channel. As activity of the cerebellar DCN

and PC neurons is involved in movement behavior,[56; 57] our findings suggest that the p.Arg1715His change of Cav3.1 could affect motor control by altering DCN activity.

All together, these elements establish *CACNA1G* mutations as a monogenic cause of ADCA, with a recurrence of the p.Arg1715His variant and a relatively high frequency of almost 0.6%, in our cohort, after exclusion of polyglutamine expansions (~0.3% of all ADCA). The other variants detected (Table S5) could be either benign polymorphisms, variants that potentiate other ion channel variants such as loss-of-function *CACNA1A* mutations, or causative mutations. Further investigations will be needed to elucidate their effects.

Interestingly, the clinical picture in the families we describe does not include any form of epilepsy. Indeed, the p.Arg1715His variant induces a shift of activation towards positive voltages, while epilepsy-associated T-type channel variants are classically associated with a gain-of-function, through faster activation, negative shift of steady-state activation/inactivation properties, or increased protein expression.[25; 51] In agreement with these observations, *CACNA1G* KO mice are resistant to induced seizures.[42] Expectedly, a positive shift in activation properties, as in our families, should be protective or have no effect.

It is of note that, in family AAD-SAL-233, individual 14 (III-9 in Figure 2) presented with both clinical signs and pathology characteristic of Alzheimer's disease (AD). Another family member presented with ataxia and Alzheimer's type dementia, but no DNA was available for sequencing and the brain was not available. Downregulation of *CACNA1G* and Cav3.1 inhibition were recently correlated, in microarrays of human tissue, mice, and cellular models, with altered APP processing, and consequently, occurrence of AD.[58] We could not determine whether the p.Arg1715His change was related to AD in this case. Nevertheless, the co-occurrence of AD at age 83 is not unexpected.

It is interesting to notice that the variant we describe, p.Arg1715His, is modifying a highly conserved arginine in the S4 segment of the domain IV of the channel. All T-type channels share a common general membrane topology with four domain repeats, each including six transmembrane segments (S1 to S6). S4 segments,

through their positive arginine residues, are considered the voltage sensing elements, and their alteration is expected to affect the voltage dependency of the channel. A systematic mutagenesis study in Cav3.1 showed that loss of the outermost arginine residues in the voltage sensor S4 segment of domain IV affects the steady-state inactivation curve.[59] Our results establish that Arg1715, the third outermost arginine in domain IV (R3), also plays a role in Cav3.1 gating by shifting the steady-state activation curve and changing the slope of the steady-state inactivation curve. This is consistent with the observation, in Cav3.2, that the equivalent arginine to histidine change (R3), also induces a positive shift in the steady-state activation curve of the protein at pH6.5,[60] what would be expected when eliminating one of the segment S4 arginines.

In conclusion, we report three ADCA families in which a common variant affecting an arginine residue in the voltage sensor S4 segment of domain IV in Cav3.1 segregates with the disease. Genetic and electrophysiological evidence support the pathogenicity of this variant. These results underscore the prominent role of Cav3.1-mediated calcium currents in the cerebellar physiology, while previous reports on dysfunctions of this channel focused on thalamocortical relay neurons. We describe a monogenic disease caused by T-type current alteration. Our results also underscore the important role played by segment S4 of domain IV in the gating properties of Cav3.1. Finally, we provide further evidence of the importance of ion channel function in the physiopathology of cerebellar ataxia, and, in particular, of calcium-related pathways.

Supplemental Data

Supplemental Data include three figures and six tables and can be found with this article online.

Acknowledgements

The authors thank the families for their contribution, as well as the DNA and Cell Bank of the Institut du Cerveau et de la Moelle épinière and the Brain Bank GIE NeuroCEB (funded by Institut Hospitalo-Universitaire A-ICM and by private foundations France Alzheimer, France Parkinson, Association de Recherche sur la Sclérose en Plaques and Connaitre les Syndromes Cérébelleux). The authors also thank Célia Gautier for her help to this study as well as Drs. Stephan Klebe, Chantal Tallaksen and Imed Féki for examining patients. MC was the recipient of a fellowship from the Fond National de la Recherche Scientifique (aspirant FNRS). This work was supported financially by the French National Agency for Research (ANR, to G.S.), the French Ministry of Health (PHRC 2009, AOM 09178, to A.D.), the European Union (Omics call: NEUROMICS, to A.Brice and A.D.), the Verum Foundation (to A.Brice and G.S.), the Fondation Roger de Spoelberch (to A.Brice), the Association Connaitre les syndromes cérébelleux (to G.S.), the program Investissements d'avenir ANR-10-IAIHU-06 (to the ICM Institute), and the Associazione Italiana Sindromi Atassiche (to ABrusco).

Table 1. Clinical characteristics of affected individuals from families AAD-SAL-233, AAD-GRE-319, and AAD-SAL-454

Individual N°* (sex)	AAD-SAL-233-9, III-3 (F)	AAD-SAL-233-14, III-9 (F)	AAD-SAL-233-20, IV-4 (M)	AAD-SAL-233-25, IV-16 (F)		AAD-SAL-233-45, V-5 (F)		AAD-SAL-233-46, V-6 (F)	AAD-GRE-319-12, II-2 (F)			AAD-GRE-319-13, III-2 (M)	AAD-GRE-319-14, II-1 (F)	AAD-SAL-454-10, III-1 (M)	
Age at exam (years)	73 (1998)	82 (2012)	43 (1999)	42 (1999)	53 (2012)	28 (2001)	39 (2012)	32 (2009)	57 (1998)	69 (2012)	72-74 (2013-2015)	51 (2015)	79 (2015)	37 (2000)	47 (2010)
Age at onset (years)	20	68	41	9		19		18	37			40	78	30	
Disease duration (years)	53	14	2	33	41	9	20	18	20	32	35-37	11	1	7	17
Symptoms at onset	Vertigo	Gait instability	Gait instability	Gait instability, vertigo		Gait instability		Gait instability	Gait instability			Gait instability	Gait instability	Gait instability	
Disability score	4/7	4/7	1/7	3/7	3/7	2/7	2/7	2/7	4/7	5/7	5/7	3/7	2/7	2/7	3/7
Cerebellar syndrome (SARA score)	Moderate	Yes	Mild	Mild	Yes (20/40)	Yes	Mild (12.5/40)	Mild	Yes	Yes (21/40)	20.5/40	12/40	4/40	Yes	Yes (12/40)
Cerebellar signs UL	Yes	NA	No	No	Yes	No	Yes	Yes	No	Mild	Mild	Mild	No	No	Yes
Dysarthria	Severe	No	Yes	Yes	Yes	No	Yes	Yes	Yes	Moderate	Moderate	Moderate	No	Yes	Yes

Ocular signs	Limited upward gaze	NA	None	Intermittent diplopia	Hypometric saccades, square waves	Saccadic pursuit	Hypometric saccades	None	Saccadic pursuit	Saccadic pursuit	Saccadic pursuit, diplopia, strabism	Saccadic pursuit	Saccadic pursuit	Nystagmus	Nystagmus
LL reflexes	+ (Ankle-)	NA	++	++	++	+	+	N	+	N	+	N	N	N	N
Spastic gait	No	NA	Mild	Mild	Mild		No	No		No	Mild	No	No	No	No
UL reflexes	N	NA	++	++	++	N	+	N	+	N	+	N	N	N	N
Babinski sign	No	NA	No	Yes	Yes	No	No	No	Unilateral	No	No	No	No	Yes	No
Decreased vibration sense at ankles	Yes	NA	Yes	No	No	No	Yes	No	No	Mild	Mild	No	Mild	No	Yes
Urinary symptoms	Urgency	NA	No	No	Incontinence	No	No	No	No	No	Urgency	No; erectile dysfunction	Urgency	Urgency	Incontinence
Other Signs	No	NA	No	No (Myokymia orbicular)	Postural UL and head tremor	No	No	No (Myokymia orbicular)	Scoliosis, Swallowing difficulties	Myokymia orbicular	Dysphagia, dysarthria	Dysphagia, dysarthria	No	No	Swallowing difficulties, Psoriasis
Mood or Cognitive impairment	No	Alzheimer's disease	Depression	Depression	No	No	N	No	No	No	No	No	No	MMS 25/30, Depression	No

Cerebral MRI	NA	NA	Vermian atrophy less foliation of the hemispheres, N-acétyl-aspartate decrease	Vermian atrophy	NA	Vermian atrophy	NA	NA	Vermian atrophy	NA	Cerebellar atrophy (vermian++), white matter hypersignals	NA	NA	Vermian Atrophy	Cerebellar and brainstem hypoplasia and atrophy

F: female

M: male

NA: not available

LL: lower limbs

UL: upper limbs

N: normal

MMS: mini mental state

MRI: magnetic resonance imaging

SDFS score: Spinocerebellar Degeneration Functional Score

0: no functional handicap; 1: no functional handicap but signs at examination; 2: mild, able to run; 3: moderate, unable to run; 4: severe, walking with one stick, unlimited walking; 5: walking with two sticks; 6: unable to walk, requiring a wheelchair; 7: bedridden

SARA score: Scale for the Assessment and Rating of Ataxia

*Personal numbers are followed by pedigree numbers according to figure 2.

Figure 1. Neuropathologic examination of the cerebellum of individual AAD-SAL-233-14 (III-9 in Figure 2)

(A - B) Case; (C - D) Control. Hematoxylin and eosin staining.
(A and C) Granular layer of the cerebellum. The black arrows in (C) point to normal glomeruli; normal glomeruli cannot be identified in (A).
(B and D) Purkinje cell layer. Four normal Purkinje cells are visible in (D), one of which is indicated by a black arrow; Purkinje cell loss is severe in (B), only the processes of the basket cells are visible ("empty baskets", black arrows). Note the additional layer composed of Bergmann glia (white arrows). The asterisk in (B) and (D) indicates the molecular layer, which appears loosened in (B).

Figure 2. Segregation of the p.Arg1715His change in ADCA pedigrees and alignment of orthologs and paralogs

(A) Pedigrees of ADCA families with the p.Arg1715His change. Number of affected individuals tested: six in AAD-SAL-233, three in AAD-GRE-319, one in AAD-SAL-454. All affected but no unaffected individuals harbor the variant in the heterozygous state.
(B) Chromatograms showing the mutation in individuals AAD-SAL-233-9 (III-3), AAD-GRE-319-12 (II-2), and AAD-SAL-454-10 (III-1).
(C) Schematic representation of Cav3.1, showing its organization in four domains, each containing six transmembrane segments; segment S4 contains many positively charged aminoacids, such as arginine, and is therefore the voltage-sensor. The p.Arg1715His change is located in segment S4 of domain IV. Alignment of orthologs (D) and paralogs (E) shows that the arginine residues in Cav3.1 are very highly conserved across all species, T-type channels, and domains.

Figure 3. Electrophysiological analysis of WT and p.Arg1715His Cav3.1 calcium channels

(A) Current traces obtained with wild-type (WT) and p.Arg1715His channels at various membrane potentials (-90, -80, -70, -65, -60, -55, -50, -45, -40, -35, -30, -25, -20 mV) and from a holding potential of -100mV. Notice the trace in red (-50mV), which shows a smaller current for the pArg1715His channel (36% of the maximum current compared with 54% for the WT)

(B) Averaged current-voltage relationships from traces in panel A. The normalized conductance-voltage curve fitted with a Boltzman equation: $I/Imax=Gmax(Vm-Erev)/(1+exp(V_{1/2}-Vm)/k)$ for each individual cell.

(C) Steady-state inactivation curves. The curves were fitted using $I/Imax=1/(1+exp(Vm—V_{1/2})/k)$

(D) Availability of calcium currents (mean steady-state activation and inactivation curves). The steady-state activation curves were fitted with a Boltzmann equation $G/Gmax=1/(1+exp(V_{1/2}-Vm)/K)$ were G was calculated as follows: G=I/(Vm-Erev).

(E and F) Time-constant of inactivation (τ inact) and activation (τ act) kinetics. The values were obtained by fitting the traces showed in panel A with a double exponential function.

(G) Recovery from short-term inactivation using a two paired-pulse protocol

(H) Deactivation kinetics (τ deact).

(I) Simulation of a DCN neuron firing using the steady state activation and inactivation values obtained for the WT (black) and the p.Arg1715His (red) channels. The DCN model used was developed by Luthman et al.[23] using the NEURON simulation environment (https://www.neuron.yale.edu/neuron/), based on the model originally implemented in GENESIS by Steuber et al.[61] The NaP, HCN and CaLVA conductances were changed to match the "Neuron 1" model described by Steuber et al.[61]

In the above-mentioned equations, $V_{1/2}$ represents either the half-activation potential (steady-state activation curve) or the half-inactivation potential (steady-state inactivation curve). Other parameters are Vm, membrane potential; Erev, reversal potential; k, slope factor; G, conductance; Gmax, maximum conductance; I, current at a given Vm; Imax, maximum current. The extracellular solution contained (in mM): 135 NaCl, 20 TEACl, 2 $CaCl_2$, 1 $MgCl_2$, 10 HEPES, pH adjusted to 7.44 with KOH. Patch pipettes were filled with an internal solution (140 mM CsCl, 10 mM EGTA, 3

mM $CaCl_2$, 10 mM HEPES, 3 mM Mg-ATP, 0.6 mM GTP, pH adjusted to 7.25 with KOH) and had a typical resistance of 2-3MΩ. From B to H: WT values are represented with black circles and p.Arg1715His with red squares. Data are represented as mean ± SEM.

Web Resources

The URLs for data presented herein are as follows:

dbSNP137, http://www.ncbi.nlm.nih.gov/projects/SNP

Exome Aggregation Consortium, http://exac.broadinstitute.org

Exome Variant Server, http://evs.gs.washington.edu/EVS/

Online Mendelian Inheritance in Man (OMIM), http://www.omim.org

Scale for the Assessment and Rating of Ataxia, http://www.ataxia-study-group.net/html/about/ataxiascales/sara/SARA.pdf

SPATAX, https://spatax.wordpress.com/

References

1. Matilla-Duenas, A., Ashizawa, T., Brice, A., Magri, S., McFarland, K.N., Pandolfo, M., Pulst, S.M., Riess, O., Rubinsztein, D.C., Schmidt, J., et al. (2014). Consensus paper: pathological mechanisms underlying neurodegeneration in spinocerebellar ataxias. Cerebellum *13*, 269-302.
2. Durr, A. (2010). Autosomal dominant cerebellar ataxias: polyglutamine expansions and beyond. Lancet Neurol. *9*, 885-894.
3. Hersheson, J., Haworth, A., and Houlden, H. (2012). The inherited ataxias: genetic heterogeneity, mutation databases, and future directions in research and clinical diagnostics. Hum. Mutat. *33*, 1324-1332.
4. Coutelier, M., Stevanin, G., and Brice, A. (2015). Genetic landscape remodelling in spinocerebellar ataxias: the influence of next-generation sequencing. J. Neurol. Published online April 11, 2015 . http://dx.doi.org/10.1007/s00415-015-7725-4.
5. Giunti, P., Mantuano, E., Frontali, M., and Veneziano, L. (2015). Molecular mechanism of Spinocerebellar Ataxia type 6: glutamine repeat disorder, channelopathy and transcriptional dysregulation. The multifaceted aspects of a single mutation. Front. Cell. Neurosci. *9*, 36.
6. Rajakulendran, S., Kaski, D., and Hanna, M.G. (2012). Neuronal P/Q-type calcium channel dysfunction in inherited disorders of the CNS. Nat. Rev. Neurol. *8*, 86-96.
7. Yan, H., Pablo, J.L., and Pitt, G.S. (2013). FGF14 regulates presynaptic Ca2+ channels and synaptic transmission. Cell. Rep. *4*, 66-75.
8. Waters, M.F., Minassian, N.A., Stevanin, G., Figueroa, K.P., Bannister, J.P., Nolte, D., Mock, A.F., Evidente, V.G., Fee, D.B., Muller, U., et al. (2006). Mutations in voltage-gated potassium channel KCNC3 cause degenerative and developmental central nervous system phenotypes. Nat. Genet. *38*, 447-451.
9. Duarri, A., Jezierska, J., Fokkens, M., Meijer, M., Schelhaas, H.J., den Dunnen, W.F., van Dijk, F., Verschuuren-Bemelmans, C., Hageman, G., van de Vlies, P., et al. (2012). Mutations in potassium channel kcnd3 cause spinocerebellar ataxia type 19. Ann. Neurol. *72*, 870-880.

10. Lee, Y.C., Durr, A., Majczenko, K., Huang, Y.H., Liu, Y.C., Lien, C.C., Tsai, P.C., Ichikawa, Y., Goto, J., Monin, M.L., et al. (2012). Mutations in KCND3 cause spinocerebellar ataxia type 22. Ann. Neurol. *72*, 859-869.
11. Hills, L.B., Masri, A., Konno, K., Kakegawa, W., Lam, A.T., Lim-Melia, E., Chandy, N., Hill, R.S., Partlow, J.N., Al-Saffar, M., et al. (2013). Deletions in GRID2 lead to a recessive syndrome of cerebellar ataxia and tonic upgaze in humans. Neurology *81*, 1378-1386.
12. Coutelier, M., Burglen, L., Mundwiller, E., Abada-Bendib, M., Rodriguez, D., Chantot-Bastaraud, S., Rougeot, C., Cournelle, M.A., Milh, M., Toutain, A., et al. (2015). GRID2 mutations span from congenital to mild adult-onset cerebellar ataxia. Neurology *84*, 1751-1759.
13. Chopra, R., and Shakkottai, V.G. (2014). Translating cerebellar Purkinje neuron physiology to progress in dominantly inherited ataxia. Future Neurol. *9*, 187-196.
14. Thal, D.R., Rub, U., Orantes, M., and Braak, H. (2002). Phases of A beta-deposition in the human brain and its relevance for the development of AD. Neurology *58*, 1791-1800.
15. Braak, H., and Braak, E. (1991). Neuropathological stageing of Alzheimer-related changes. Acta Neuropathol. *82*, 239-259.
16. Samocha, K.E., Robinson, E.B., Sanders, S.J., Stevens, C., Sabo, A., McGrath, L.M., Kosmicki, J.A., Rehnstrom, K., Mallick, S., Kirby, A., et al. (2014). A framework for the interpretation of de novo mutation in human disease. Nat. Genet. *46*, 944-950.
17. Ikeda, Y., Dick, K.A., Weatherspoon, M.R., Gincel, D., Armbrust, K.R., Dalton, J.C., Stevanin, G., Durr, A., Zuhlke, C., Burk, K., et al. (2006). Spectrin mutations cause spinocerebellar ataxia type 5. Nat. Genet. *38*, 184-190.
18. Ernst, W.L., Zhang, Y., Yoo, J.W., Ernst, S.J., and Noebels, J.L. (2009). Genetic enhancement of thalamocortical network activity by elevating alpha 1g-mediated low-voltage-activated calcium current induces pure absence epilepsy. J. Neurosci. *29*, 1615-1625.
19. Ly, R., Bouvier, G., Schonewille, M., Arabo, A., Rondi-Reig, L., Lena, C., Casado, M., De Zeeuw, C.I., and Feltz, A. (2013). T-type channel blockade impairs long-term potentiation at the parallel fiber-Purkinje cell synapse and cerebellar learning. Proc. Natl. Acad. Sci. USA *110*, 20302-20307.
20. Talley, E.M., Cribbs, L.L., Lee, J.H., Daud, A., Perez-Reyes, E., and Bayliss, D.A. (1999). Differential distribution of three members of a gene family encoding low voltage-activated (T-type) calcium channels. J. Neurosci. *19*, 1895-1911.
21. Monteil, A., Chemin, J., Bourinet, E., Mennessier, G., Lory, P., and Nargeot, J. (2000). Molecular and functional properties of the human alpha(1G) subunit that forms T-type calcium channels. J. Biol. Chem. *275*, 6090-6100.
22. Engbers, J.D., Anderson, D., Zamponi, G.W., and Turner, R.W. (2013). Signal processing by T-type calcium channel interactions in the cerebellum. Front. Cell. Neurosci. *7*, 230.
23. Luthman, J., Hoebeek, F.E., Maex, R., Davey, N., Adams, R., De Zeeuw, C.I., and Steuber, V. (2011). STD-dependent and independent encoding of input irregularity as spike rate in a computational model of a cerebellar nucleus neuron. Cerebellum *10*, 667-682.

24. Perez-Reyes, E. (2006). Molecular characterization of T-type calcium channels. Cell Calcium *40*, 89-96.
25. Cain, S.M., and Snutch, T.P. (2011). Voltage-gated calcium channels and disease. Biofactors *37*, 197-205.
26. Simms, B.A., and Zamponi, G.W. (2014). Neuronal voltage-gated calcium channels: structure, function, and dysfunction. Neuron *82*, 24-45.
27. Hamid, J., Peloquin, J.B., Monteil, A., and Zamponi, G.W. (2006). Determinants of the differential gating properties of Cav3.1 and Cav3.3 T-type channels: a role of domain IV? Neuroscience *143*, 717-728.
28. Chen, D.H., Brkanac, Z., Verlinde, C.L., Tan, X.J., Bylenok, L., Nochlin, D., Matsushita, M., Lipe, H., Wolff, J., Fernandez, M., et al. (2003). Missense mutations in the regulatory domain of PKC gamma: a new mechanism for dominant nonepisodic cerebellar ataxia. Am. J. Hum. Genet. *72*, 839-849.
29. Chemin, J., Monteil, A., Perez-Reyes, E., Bourinet, E., Nargeot, J., and Lory, P. (2002). Specific contribution of human T-type calcium channel isotypes (alpha(1G), alpha(1H) and alpha(1I)) to neuronal excitability. J. Physiol. *540*, 3-14.
30. Molineux, M.L., McRory, J.E., McKay, B.E., Hamid, J., Mehaffey, W.H., Rehak, R., Snutch, T.P., Zamponi, G.W., and Turner, R.W. (2006). Specific T-type calcium channel isoforms are associated with distinct burst phenotypes in deep cerebellar nuclear neurons. Proc. Natl. Acad. Sci. USA *103*, 5555-5560.
31. Crunelli, V., Toth, T.I., Cope, D.W., Blethyn, K., and Hughes, S.W. (2005). The 'window' T-type calcium current in brain dynamics of different behavioural states. J. Physiol. *562*, 121-129.
32. Perez-Reyes, E. (2003). Molecular physiology of low-voltage-activated t-type calcium channels. Physiol. Rev. *83*, 117-161.
33. Chemin, J., Monteil, A., Briquaire, C., Richard, S., Perez-Reyes, E., Nargeot, J., and Lory, P. (2000). Overexpression of T-type calcium channels in HEK-293 cells increases intracellular calcium without affecting cellular proliferation. FEBS Lett. *478*, 166-172.
34. Shin, H.S., Cheong, E.J., Choi, S., Lee, J., and Na, H.S. (2008). T-type Ca2+ channels as therapeutic targets in the nervous system. Curr. Opin. Pharmacol. *8*, 33-41.
35. Yalcin, O. (2012). Genes and molecular mechanisms involved in the epileptogenesis of idiopathic absence epilepsies. Seizure *21*, 79-86.
36. Craig, P.J., Beattie, R.E., Folly, E.A., Banerjee, M.D., Reeves, M.B., Priestley, J.V., Carney, S.L., Sher, E., Perez-Reyes, E., and Volsen, S.G. (1999). Distribution of the voltage-dependent calcium channel alpha1G subunit mRNA and protein throughout the mature rat brain. Eur. J. Neurosci. *11*, 2949-2964.
37. Molineux, M.L., Mehaffey, W.H., Tadayonnejad, R., Anderson, D., Tennent, A.F., and Turner, R.W. (2008). Ionic factors governing rebound burst phenotype in rat deep cerebellar neurons. J. Neurophysiol. *100*, 2684-2701.
38. Alvina, K., Ellis-Davies, G., and Khodakhah, K. (2009). T-type calcium channels mediate rebound firing in intact deep cerebellar neurons. Neuroscience *158*, 635-641.
39. Engbers, J.D., Anderson, D., Tadayonnejad, R., Mehaffey, W.H., Molineux, M.L., and Turner, R.W. (2011). Distinct roles for I(T) and I(H) in controlling the

frequency and timing of rebound spike responses. J. Physiol. *589*, 5391-5413.
40. Engbers, J.D., Anderson, D., Asmara, H., Rehak, R., Mehaffey, W.H., Hameed, S., McKay, B.E., Kruskic, M., Zamponi, G.W., and Turner, R.W. (2012). Intermediate conductance calcium-activated potassium channels modulate summation of parallel fiber input in cerebellar Purkinje cells. Proc. Natl. Acad. Sci. USA *109*, 2601-2606.
41. Womack, M.D., and Khodakhah, K. (2004). Dendritic control of spontaneous bursting in cerebellar Purkinje cells. J. Neurosci. *24*, 3511-3521.
42. Kim, D., Song, I., Keum, S., Lee, T., Jeong, M.J., Kim, S.S., McEnery, M.W., and Shin, H.S. (2001). Lack of the burst firing of thalamocortical relay neurons and resistance to absence seizures in mice lacking alpha(1G) T-type Ca(2+) channels. Neuron *31*, 35-45.
43. Chang, K.Y., Park, Y.G., Park, H.Y., Homanics, G.E., Kim, J., and Kim, D. (2011). Lack of CaV3.1 channels causes severe motor coordination defects and an age-dependent cerebellar atrophy in a genetic model of essential tremor. Biochem. Biophys. Res. Commun. *410*, 19-23.
44. Lee, J., Kim, D., and Shin, H.S. (2004). Lack of delta waves and sleep disturbances during non-rapid eye movement sleep in mice lacking alpha1G-subunit of T-type calcium channels. Proc. Natl. Acad. Sci. USA *101*, 18195-18199.
45. Na, H.S., Choi, S., Kim, J., Park, J., and Shin, H.S. (2008). Attenuated neuropathic pain in Cav3.1 null mice. Mol. Cells *25*, 242-246.
46. Mangoni, M.E., Traboulsie, A., Leoni, A.L., Couette, B., Marger, L., Le Quang, K., Kupfer, E., Cohen-Solal, A., Vilar, J., Shin, H.S., et al. (2006). Bradycardia and slowing of the atrioventricular conduction in mice lacking CaV3.1/alpha1G T-type calcium channels. Circ. Res. *98*, 1422-1430.
47. Bidaud, I., and Lory, P. (2011). Hallmarks of the channelopathies associated with L-type calcium channels: a focus on the Timothy mutations in Ca(v)1.2 channels. Biochimie *93*, 2080-2086.
48. Chen, Y., Lu, J., Pan, H., Zhang, Y., Wu, H., Xu, K., Liu, X., Jiang, Y., Bao, X., Yao, Z., et al. (2003). Association between genetic variation of CACNA1H and childhood absence epilepsy. Ann. Neurol. *54*, 239-243.
49. Heron, S.E., Phillips, H.A., Mulley, J.C., Mazarib, A., Neufeld, M.Y., Berkovic, S.F., and Scheffer, I.E. (2004). Genetic variation of CACNA1H in idiopathic generalized epilepsy. Ann. Neurol. *55*, 595-596.
50. Khosravani, H., Altier, C., Simms, B., Hamming, K.S., Snutch, T.P., Mezeyova, J., McRory, J.E., and Zamponi, G.W. (2004). Gating effects of mutations in the Cav3.2 T-type calcium channel associated with childhood absence epilepsy. J. Biol. Chem. *279*, 9681-9684.
51. Eckle, V.S., Shcheglovitov, A., Vitko, I., Dey, D., Yap, C.C., Winckler, B., and Perez-Reyes, E. (2014). Mechanisms by which a CACNA1H mutation in epilepsy patients increases seizure susceptibility. J. Physiol. *592*, 795-809.
52. Singh, B., Monteil, A., Bidaud, I., Sugimoto, Y., Suzuki, T., Hamano, S., Oguni, H., Osawa, M., Alonso, M.E., Delgado-Escueta, A.V., et al. (2007). Mutational analysis of CACNA1G in idiopathic generalized epilepsy. Mutation in brief #962. Online. Hum. Mutat. *28*, 524-525.
53. Strom, S.P., Stone, J.L., Ten Bosch, J.R., Merriman, B., Cantor, R.M., Geschwind, D.H., and Nelson, S.F. (2010). High-density SNP association study of the

17q21 chromosomal region linked to autism identifies CACNA1G as a novel candidate gene. Mol. Psychiatry *15*, 996-1005.
54. Najmabadi, H., Hu, H., Garshasbi, M., Zemojtel, T., Abedini, S.S., Chen, W., Hosseini, M., Behjati, F., Haas, S., Jamali, P., et al. (2011). Deep sequencing reveals 50 novel genes for recessive cognitive disorders. Nature *478*, 57-63.
55. Tscherter, A., David, F., Ivanova, T., Deleuze, C., Renger, J.J., Uebele, V.N., Shin, H.S., Bal, T., Leresche, N., and Lambert, R.C. (2011). Minimal alterations in T-type calcium channel gating markedly modify physiological firing dynamics. J. Physiol. *589*, 1707-1724.
56. Heiney, S.A., Wohl, M.P., Chettih, S.N., Ruffolo, L.I., and Medina, J.F. (2014). Cerebellar-dependent expression of motor learning during eyeblink conditioning in head-fixed mice. J. Neurosci. *34*, 14845-14853.
57. Witter, L., Canto, C.B., Hoogland, T.M., de Gruijl, J.R., and De Zeeuw, C.I. (2013). Strength and timing of motor responses mediated by rebound firing in the cerebellar nuclei after Purkinje cell activation. Front. Neural Circuits *7*, 133.
58. Rice, R.A., Berchtold, N.C., Cotman, C.W., and Green, K.N. (2014). Age-related downregulation of the CaV3.1 T-type calcium channel as a mediator of amyloid beta production. Neurobiol. Aging *35*, 1002-1011.
59. Kurejova, M., Lacinova, L., Pavlovicova, M., Eschbach, M., and Klugbauer, N. (2007). The effect of the outermost basic residues in the S4 segments of the Ca(V)3.1 T-type calcium channel on channel gating. Pflugers Arch. *455*, 527-539.
60. Lam, A.D., Chikina, M.D., McNulty, M.M., Glaaser, I.W., and Hanck, D.A. (2005). Role of Domain IV/S4 outermost arginines in gating of T-type calcium channels. Pflugers Arch. *451*, 349-361.
61. Steuber, V., Schultheiss, N.W., Silver, R.A., De Schutter, E., and Jaeger, D. (2011). Determinants of synaptic integration and heterogeneity in rebound firing explored with data-driven models of deep cerebellar nucleus cells. J. Comput. Neurosci. *30*, 633-658.

Table 1. Clinical characteristics of affected individuals from families AAD-SAL-233, AAD-GRE-319, and AAD-SAL-454

Individual N°* (sex)	AAD-SAL-233-9, III-3 (F)	AAD-SAL-233-14, III-9 (F)	AAD-SAL-233-20, IV-4 (M)	AAD-SAL-233-25, IV-16 (F)		AAD-SAL-233-45, V-5 (F)		AAD-SAL-233-46, V-6 (F)	AAD-GRE-319-12, II-2 (F)			AAD-GRE-319-13, III-2 (M)	AAD-GRE-319-14, II-1 (F)	AAD-SAL-454-10, III-1 (M)	
Age at exam (years)	73 (1998)	82 (2012)	43 (1999)	42 (1999)	53 (2012)	28 (2001)	39 (2012)	32 (2009)	57 (1998)	69 (2012)	72-74 (2013-2015)	51 (2015)	79 (2015)	37 (2000)	47 (2010)
Age at onset (years)	20	68	41	9		19		18	37			40	78	30	
Disease duration (years)	53	14	2	33	41	9	20	18	20	32	35-37	11	1	7	17
Symptoms at onset	Vertigo	Gait instability	Gait instability	Gait instability, vertigo		Gait instability		Gait instability	Gait instability			Gait instability	Gait instability	Gait instability	
Disability score	4/7	4/7	1/7	3/7	3/7	2/7	2/7	2/7	4/7	5/7	5/7	3/7	2/7	2/7	3/7
Cerebellar syndrome (SARA score)	Moderate	Yes	Mild	Mild	Yes (20/40)	Yes	Mild (12.5/40)	Mild	Yes	Yes (21/40)	20.5/40	12/40	4/40	Yes	Yes (12/40)
Cerebellar signs UL	Yes	NA	No	No	Yes	No	Yes	Yes	No	Mild	Mild	Mild	No	No	Yes
Dysarthria	Severe	No	Yes	Yes	Yes	No	Yes	Yes	Yes	Moderate	Moderate	Moderate	No	Yes	Yes

Ocular signs	Limited upward gaze	NA	None	Intermittent diplopia	Hypometric saccades, square waves	Saccadic pursuit	Hypometric saccades	None	Saccadic pursuit	Saccadic pursuit	Saccadic pursuit, diplopia, strabism	Saccadic pursuit	Saccadic pursuit	Nystagmus	Nystagmus
LL reflexes	+ (Ankle-)	NA	++	++	++	+	+	N	+	N	+	N	N	N	N
Spastic gait	No	NA	Mild	Mild	Mild		No	No		No	Mild	No	No	No	No
UL reflexes	N	NA	++	++	++	N	+	N	+	N	+	N	N	N	N
Babinski sign	No	NA	No	Yes	Yes	No	No	No	Unilateral	No	No	No	No	Yes	No
Decreased vibration sense at ankles	Yes	NA	Yes	No	No	No	Yes	No	No	Mild	Mild	No	Mild	No	Yes
Urinary symptoms	Urgency	NA	No	No	Incontinence	No	No	No	No	No	Urgency	No; erectile dysfunction	Urgency	Urgency	Incontinence
Other Signs	No	NA	No	No (Myokymia orbicular)	Postural UL and head tremor	No	No	No (Myokymia orbicular)	Scoliosis, Swallowing difficulties	Myokymia orbicular	Dysphagia, dysarthria	Dysphagia, dysarthria	No	No	Swallowing difficulties, Psoriasis
Mood or Cognitive impairment	No	Alzheimer's disease	Depression	Depression	No	No	N	No	No	No	No	No	No	MMS 25/30, Depression	No

Cerebral MRI	NA	NA	Vermian atrophy less foliation of the hemispheres, N-acétyl-aspartate decrease	Vermian atrophy	NA	Vermian atrophy	NA	NA	Vermian atrophy	NA	Cerebellar atrophy (vermian++), white matter hypersignals	NA	NA	Vermian Atrophy	Cerebellar and brainstem hypoplasia and atrophy

F: female

M: male

NA: not available

LL: lower limbs

UL: upper limbs

N: normal

MMS: mini mental state

MRI: magnetic resonance imaging

SDFS score: Spinocerebellar Degeneration Functional Score

0: no functional handicap; 1: no functional handicap but signs at examination; 2: mild, able to run; 3: moderate, unable to run; 4: severe, walking with one stick, unlimited walking; 5: walking with two sticks; 6: unable to walk, requiring a wheelchair; 7: bedridden

SARA score: Scale for the Assessment and Rating of Ataxia

*Personal numbers are followed by pedigree numbers according to figure 2.

Figure 1. Neuropathologic examination of the cerebellum of individual AAD-SAL-233-14 (III-9 in Figure 2)

(A - B) Case; (C - D) Control. Hematoxylin and eosin staining.
(A and C) Granular layer of the cerebellum. The black arrows in (C) point to normal glomeruli; normal glomeruli cannot be identified in (A).
(B and D) Purkinje cell layer. Four normal Purkinje cells are visible in (D), one of which is indicated by a black arrow; Purkinje cell loss is severe in (B), only the processes of the basket cells are visible ("empty baskets", black arrows). Note the additional layer composed of Bergmann glia (white arrows). The asterisk in (B) and (D) indicates the molecular layer, which appears loosened in (B).

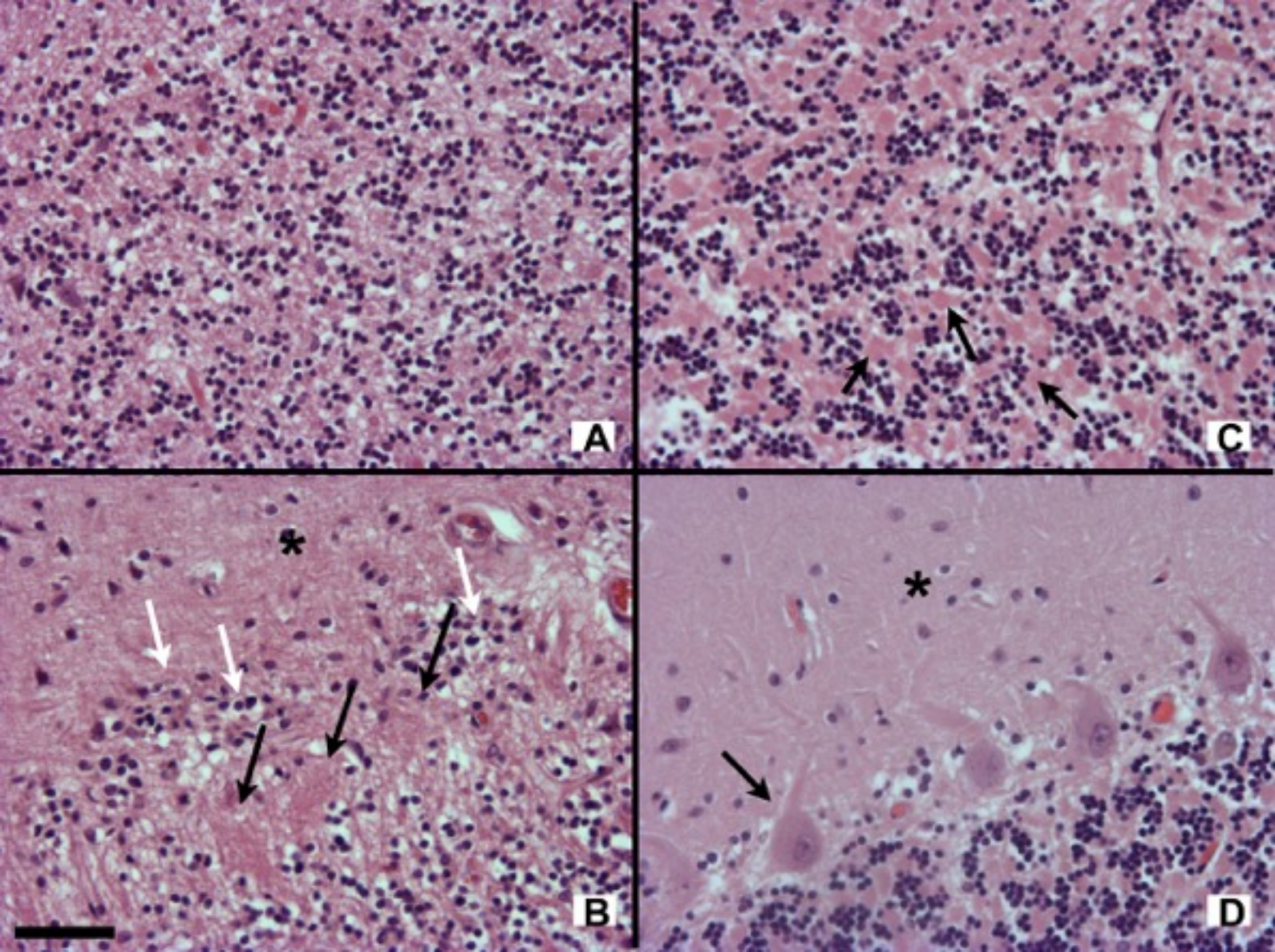
A
C
B
D

Figure 2. Segregation of the p.Arg1715His change in ADCA pedigrees and alignment of orthologs and paralogs

(A) Pedigrees of ADCA families with the p.Arg1715His change. Number of affected individuals tested: six in AAD-SAL-233, three in AAD-GRE-319, one in AAD-SAL-454. All affected but no unaffected individuals harbor the variant in the heterozygous state.
(B) Chromatograms showing the mutation in individuals AAD-SAL-233-9 (III-3), AAD-GRE-319-12 (II-2), and AAD-SAL-454-10 (III-1).
(C) Schematic representation of Cav3.1, showing its organization in four domains, each containing six transmembrane segments; segment S4 contains many positively charged aminoacids, such as arginine, and is therefore the voltage-sensor. The p.Arg1715His change is located in segment S4 of domain IV. Alignment of orthologs (D) and paralogs (E) shows that the arginine residues in Cav3.1 are very highly conserved across all species, T-type channels, and domains.

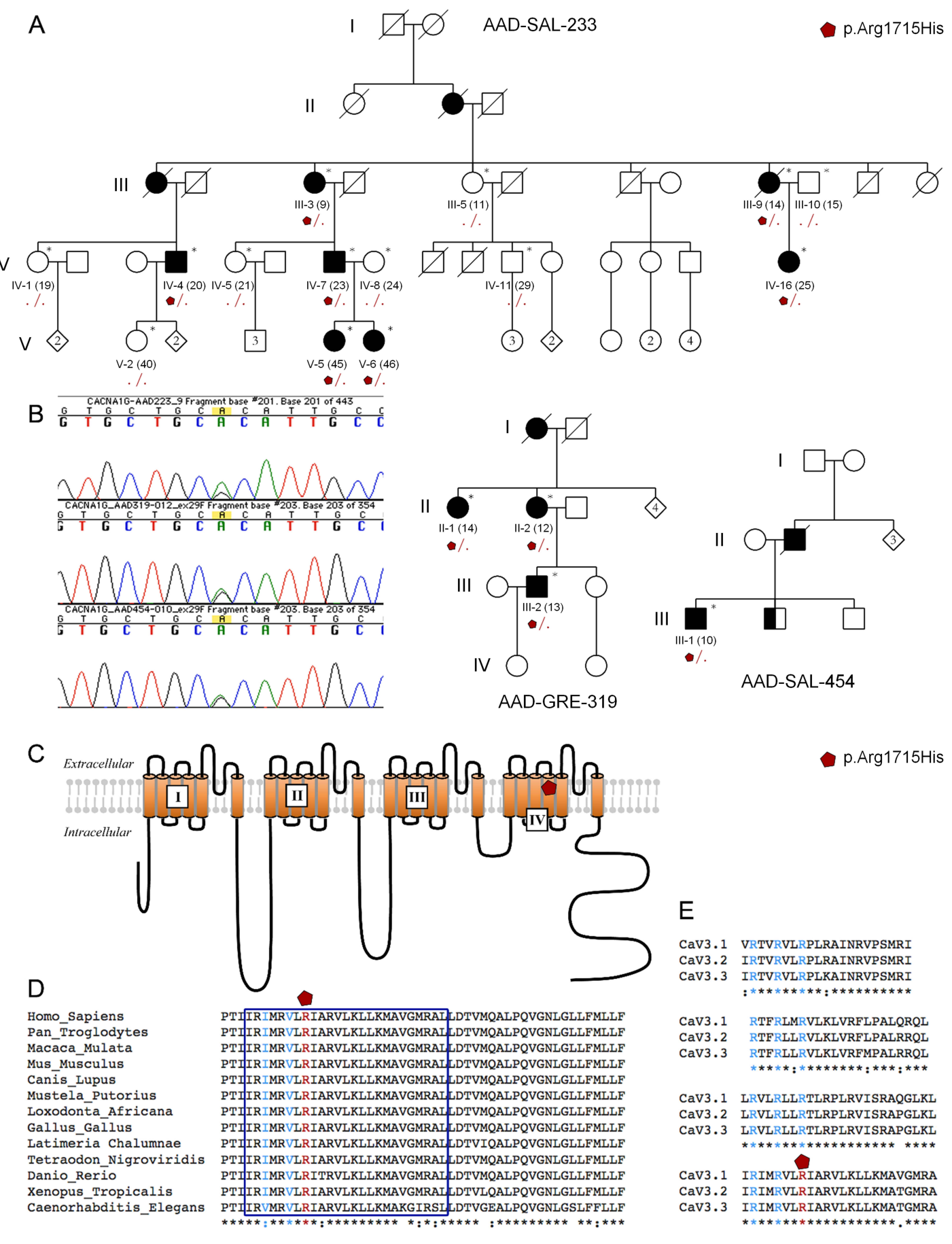
A
AAD-SAL-233
p.Arg1715His
I
II
III
III-3 (9)
III-5 (11)
III-9 (14)
III-10 (15)
IV-1 (19)
IV-4 (20)
IV-5 (21)
IV-7 (23)
IV-8 (24)
IV-11 (29)
IV-16 (25)
V-2 (40)
V-5 (45)
V-6 (46)
B
CACNA1G-AAD223_9 Fragment base #201. Base 201 of 443
CACNA1G_AAD319-012_ex29F Fragment base #203. Base 203 of 354
CACNA1G_AAD454-010_ex29F Fragment base #203. Base 203 of 354
II-1 (14)
II-2 (12)
III-2 (13)
AAD-GRE-319
III-1 (10)
AAD-SAL-454
C
Extracellular
Intracellular
p.Arg1715His
D
Homo_Sapiens PTIIRIMRVLRIARVLKLLKMAVGMRALLDTVMQALPQVGNLGLLFMLLF
Pan_Troglodytes PTIIRIMRVLRIARVLKLLKMAVGMRALLDTVMQALPQVGNLGLLFMLLF
Macaca_Mulata PTIIRIMRVLRIARVLKLLKMAVGMRALLDTVMQALPQVGNLGLLFMLLF
Mus_Musculus PTIIRIMRVLRIARVLKLLKMAVGMRALLDTVMQALPQVGNLGLLFMLLF
Canis_Lupus PTIIRIMRVLRIARVLKLLKMAVGMRALLDTVMQALPQVGNLGLLFMLLF
Mustela_Putorius PTIIRIMRVLRIARVLKLLKMAVGMRALLDTVMQALPQVGNLGLLFMLLF
Loxodonta_Africana PTIIRIMRVLRIARVLKLLKMAVGMRALLDTVMQALPQVGNLGLLFMLLF
Gallus_Gallus PTIIRIMRVLRIARVLKLLKMAVGMRALLDTVMQALPQVGNLGLLFMLLF
Latimeria Chalumnae PTIIRIMRVLRIARVLKLLKMAVGMRALLDTVIQALPQVGNLGLLFMLLF
Tetraodon_Nigroviridis PTIIRIMRVLRIARVLKLLKMAVGMRALLDTVMQALPQVGNLGLLFMLLF
Danio_Rerio PTIIRIMRVLRITRVLKLLKMAVGMRALLDTVMQALPQVGNLGLLFMLLF
Xenopus_Tropicalis PTIIRIMRVLRIARVLKLLKMAVGMRALLDTVLQALPQVGNLGLLFMLLF
Caenorhabditis_Elegans PTIIRVMRVLRIARVLKLLKMAKGIRSLLDTVGEALPQVGNLGSLFFLLF
E
CaV3.1 VRTVRVLRPLRAINRVPSMRI
CaV3.2 IRTVRVLRPLRAINRVPSMRI
CaV3.3 IRTVRVLRPLKAINRVPSMRI
CaV3.1 RTFRLMRVLKLVRFLPALQRQL
CaV3.2 RTFRLLRVLKLVRFLPALRRQL
CaV3.3 RTFRLLRVLKLVRFMPALRRQL
CaV3.1 LRVLRLLRTLRPLRVISRAQGLKL
CaV3.2 LRVLRLLRTLRPLRVISRAPGLKL
CaV3.3 LRVLRLLRTLRPLRVISRAPGLKL
CaV3.1 IRIMRVLRIARVLKLLKMAVGMRA
CaV3.2 IRIMRVLRIARVLKLLKMATGMRA
CaV3.3 IRIMRVLRIARVLKLLKMATGMRA

Figure 3. Electrophysiological analysis of WT and p.Arg1715His Cav3.1 calcium channels

(A) Current traces obtained with wild-type (WT) and p.Arg1715His channels at various membrane potentials (-90, -80, -70, -65, -60, -55, -50, -45, -40, -35, -30, -25, -20 mV) and from a holding potential of -100mV. Notice the trace in red (-50mV), which shows a smaller current for the pArg1715His channel (36% of the maximum current compared with 54% for the WT)

(B) Averaged current-voltage relationships from traces in panel A. The normalized conductance-voltage curve fitted with a Boltzman equation: $I/Imax=Gmax(Vm-Erev)/(1+exp(V_{1/2}-Vm)/k)$ for each individual cell.

(C) Steady-state inactivation curves. The curves were fitted using $I/Imax=1/(1+exp(Vm—V_{1/2})/k)$

(D) Availability of calcium currents (mean steady-state activation and inactivation curves). The steady-state activation curves were fitted with a Boltzmann equation $G/Gmax=1/(1+exp(V_{1/2}-Vm)/K)$ were G was calculated as follows: G=I/(Vm-Erev).

(E and F) Time-constant of inactivation (τ inact) and activation (τ act) kinetics. The values were obtained by fitting the traces showed in panel A with a double exponential function.

(G) Recovery from short-term inactivation using a two paired-pulse protocol

(H) Deactivation kinetics (τ deact).

(I) Simulation of a DCN neuron firing using the steady state activation and inactivation values obtained for the WT (black) and the p.Arg1715His (red) channels. The DCN model used was developed by Luthman et al.[23] using the NEURON simulation environment (https://www.neuron.yale.edu/neuron/), based on the model originally implemented in GENESIS by Steuber et al.[61] The NaP, HCN and CaLVA conductances were changed to match the "Neuron 1" model described by Steuber et al.[61]

In the above-mentioned equations, $V_{1/2}$ represents either the half-activation potential (steady-state activation curve) or the half-inactivation potential (steady-state inactivation curve). Other parameters are Vm, membrane potential; Erev, reversal potential; k, slope factor; G, conductance; Gmax, maximum conductance; I, current at a given Vm; Imax, maximum current. The extracellular solution contained (in mM): 135 NaCl, 20 TEACl, 2 $CaCl_2$, 1 $MgCl_2$, 10 HEPES, pH adjusted to 7.44 with KOH.

Patch pipettes were filled with an internal solution (140 mM CsCl, 10 mM EGTA, 3 mM $CaCl_2$, 10 mM HEPES, 3 mM Mg-ATP, 0.6 mM GTP, pH adjusted to 7.25 with KOH) and had a typical resistance of 2-3MΩ. From B to H: WT values are represented with black circles and p.Arg1715His with red squares. Data are represented as mean ± SEM.

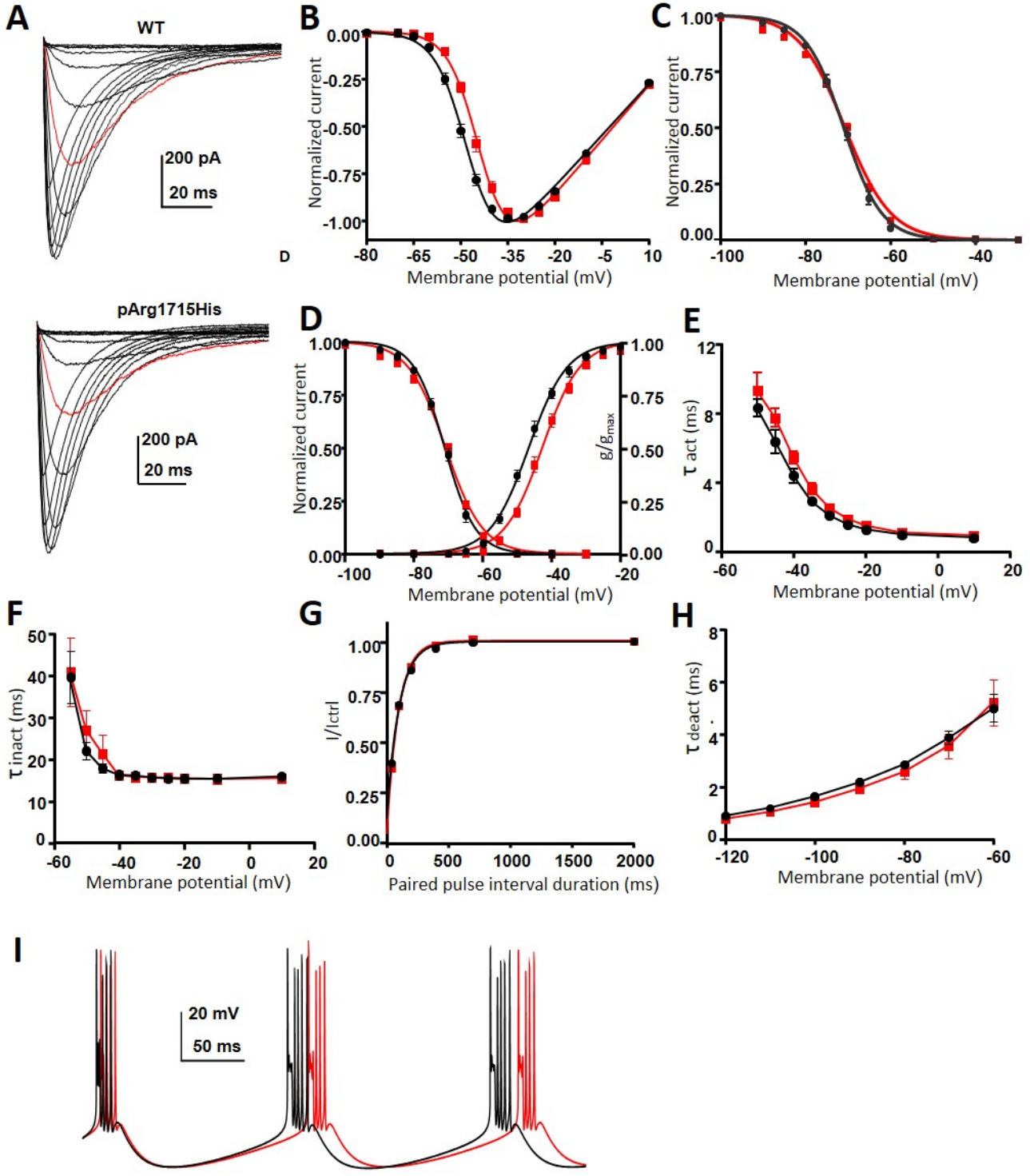
A
WT
200 pA
20 ms
B
Normalized current
Membrane potential (mV)
C
Normalized current
Membrane potential (mV)
D
pArg1715His
200 pA
20 ms
D
Normalized current
g/gmax
Membrane potential (mV)
E
τ act (ms)
Membrane potential (mV)
F
τ inact (ms)
Membrane potential (mV)
G
I/Ictrl
Paired pulse interval duration (ms)
H
τ deact (ms)
Membrane potential (mV)
I
20 mV
50 ms

Supplemental Figure S1

Figure S1. MRI findings in individual AAD-SAL-233-25 (IV-16 in Figure 2)

Cerebral MRI in individual AAD-SAL-233-25 (IV-16 in Figure 2) at age 49. Sagittal view of a T1-weighted sequence showing superior cerebellar vermian atrophy, normal pons and cerebellar amygdala.

Supplemental Figure S2

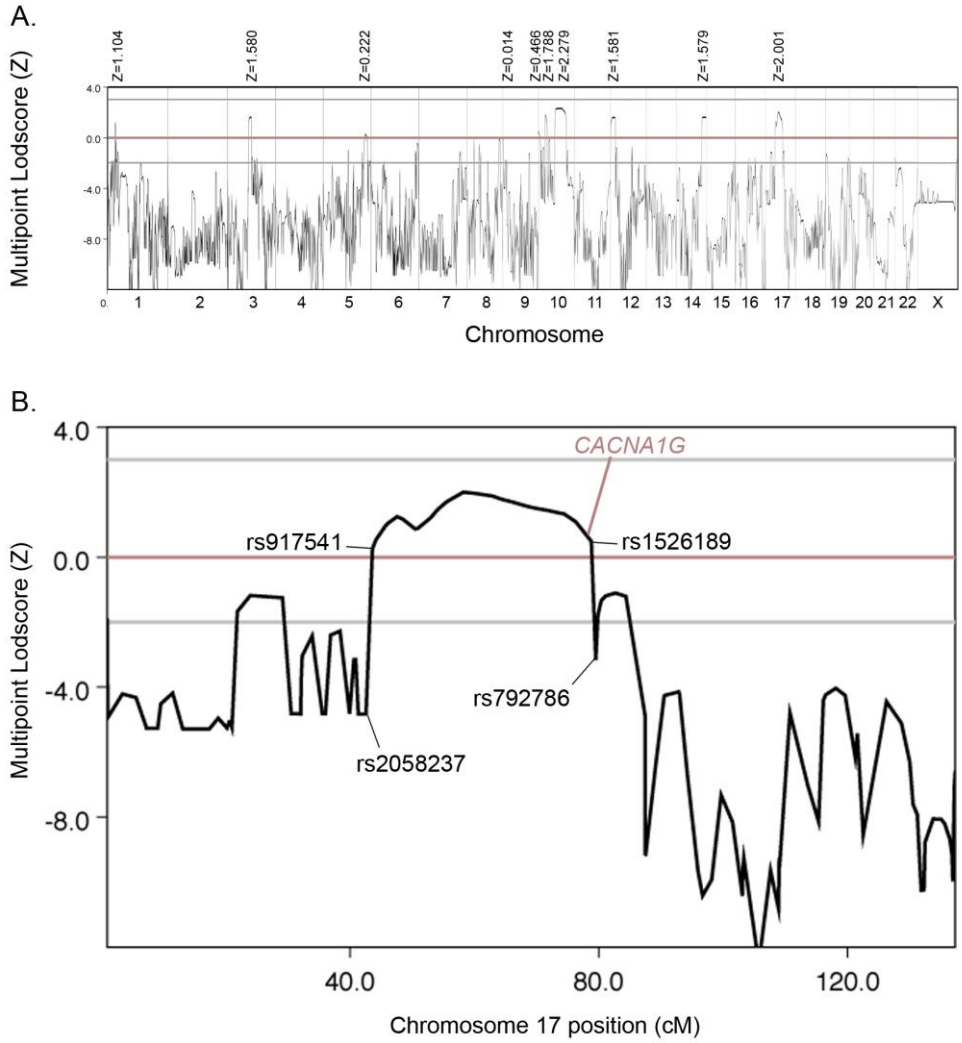

Figure S2. Whole genome linkage analysis in family AAD-SAL-233.

(A) Multipoint linkage analysis on all the autosomes in AAD-SAL-233 family. Whole genome linkage analysis was performed using Illumina LINKAGE_12 microarrays (6090 SNP markers). Genotypes were determined using Beadstudio (Illumina) and analyzed with MERLIN 1.0,[1] assuming an autosomal dominant transmission under a 0.80 penetrance model with equal allele frequencies, similar recombination fractions between males and females, and a disease frequency of 0.00001. Genotypes were available for 12 individuals, including affected subjects 9, 14, 20, 23, 25, 45, 46 (III-3, III-9, IV-4, IV-7, IV-16, V-5 and V-6 in Figure 2) and their relatives, 11, 15, 21, 24, 29 (III-5, III-10, IV-5, IV-8 and IV-11 in Figure 2). Whole genome linkage analysis could not lead to the identification of a unique well-defined associated locus due to pedigree structure and size limitations. Instead, various putatively linked or unexcluded (LOD scores above -2) loci were found in the family, including six putatively linked loci with multipoint LOD scores reaching the maximal expected values of this pedigree (from +1.579 to +2.279) and various uninformative regions. **(B)** Close-up view of the linkage analysis results for chromosome 17. A significant multipoint LOD score (Zmax = +2.001) was found between markers rs2058237 and rs792786, in a region encompassing the *CACNA1G* gene.

Supplemental Figure S3

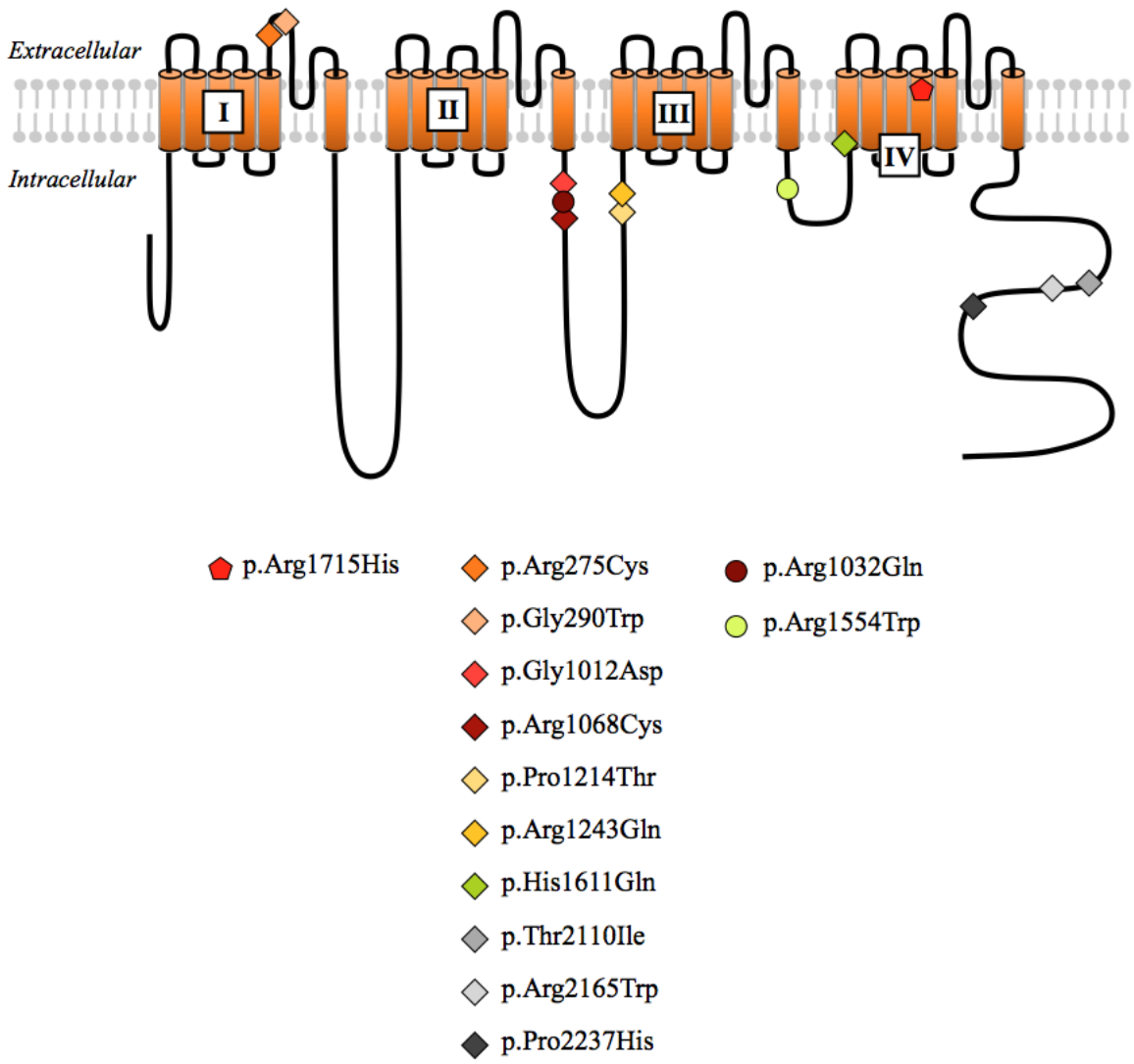

Figure S3. Schematics of Cav3.1 with other variants found by panel sequencing.

Schematics of Cav3.1 with all changes linked to *CACNA1G* variants encompassed by panel sequencing. Genetic characteristics of the variants are summarized in Table S4. The deleterious p.Arg1715His change is shown with a bright red pentagon; Variants of Unknown Significance are represented with diamonds, Variants of Unknown Significance found in individuals otherwise presenting a *CACNA1A* frameshift are indicated with circles.

Supplemental Table S1

Individual	AAD-SAL-233-15 (III-10)	AAD-SAL-233-25 (IV-16)
Number of reads	292635836	270474232
Aligned reads	291158538 (99.50%)	268296715 (99.19%)
Aligned but not duplicated reads	91598083 (31.30%)	95951959 (35.48%)
Percentage of target with >30x coverage	86.57%	85.47%
Number of variants	34226	36501
Number of variants in exons +/-200bp	31133	33083

Table S1. Whole exome sequencing statistics.

The BWA software was used in order to map reads on the reference genome: Human reference hg19. Reads related to PCR duplicates were removed from the alignment using Samtools.

Mutations were called according to the following criteria: (i) position coverage greater or equal to 20, ii) mutation proportion greater or equal to 25%, iii) mutated bases called at least 10% on each strand.

Supplemental Table S2

Chromosome	Position	Reference	Alternative	Gene	Segregation	Aminoacid change	SIFT score	Polyphen2_HDIV score	Polyphen2_HVAR score	MutationTaster score	GERP++	PhyloP 46 way	Maximal Population Frequency	1000G ALL	ExAC All	ExAC East Asian	ExAC South Asian	EVS All	EVS African American	EVS European American
10	95372766	G	A	*PDE6C*	present in all affected and healthy individual 19 (IV-1)	NM_006204.2: c.284G>A: p.Arg95His	0 (D)	0.987 (D)	0.573 (P)	D (1)	4.5	1.527	0.0003	.	0	0.0001	0.0002	0.0002	.	0.0003
17	48694921	G	A	*CACNA1G*	present in all affected, absent from all unaffected	NM_018896.4: c.5144G>A: p.Arg1715His	0 (D)	1 (D)	1 (D)	D (1)	5.02	2.348	.	.	.	.	.	.	.	.

Table S2. Characteristics of AAD-SAL-233 variants.

Summary of characteristics for both variants segregating in family AAD-SAL-233. Annotation was performed using Annovar (www.openbioinformatics.org/annovar/).[2] The database frequencies originate from 1000 genomes (www.1000genomes.org/), Exome Variant Server (EVS, http://evs.gs.washington.edu/EVS) and Exome Aggregation Consortium (ExAC, http://exac.broadinstitute.org/). Pathogenicity scores are evaluated as follows: SIFT (http://sift.jcvi.org/) predicts deleteriousness (D) under 0.05; Polyphen2 (http://genetics.bwh.harvard.edu/pph2/) classifies SNPs as probably damaging (D; HDIV>=0.957, HVAR>=0.909), possibly damaging (P; 0.453<=HDIV<=0.956, 0.447<=pp2_hdiv<=0.908), or benign (B; HDIV<=0.452, HVAR <=0.446); LRT differentiates variants with deleterious (D), neutral (N) or unknown (U) effect;[3] MutationTaster (http://www.mutationtaster.org/) classifies them as "disease_causing_automatic" (A), "disease_causing" (D), "polymorphism" (N) or "polymorphism_automatic" (P) with a given probability value, 1 being the most probable. For both GERP++ (http://mendel.stanford.edu/SidowLab/downloads/gerp/) and PhyloP (http://compgen.bscb.cornell.edu/phast/help-pages/phyloP.txt), higher scores indicate better residue conservation.

Supplemental Table S3

	PCRs / GSJunior (n=96)					Fluidigm / MiSeq (n=384)				
Exon	**Mean coverage of exon (all individuals)**	**Mean percentage of exon covered <10x**	**Number of individuals with >=10% of exon covered <10x**	**Mean percentage of exon covered >=30x**	**Number of individuals with >=90% of exon covered >=30x**	**Mean coverage of exon (all individuals)**	**Mean percentage of exon covered <10x**	**Number of individuals with >=10% of exon covered <10x**	**Mean percentage of exon covered >=30x**	**Number of individuals with >=90% of exon covered >=30x**
1	70.1	23.9	23	38.3	36	0.1	99.9	384	0	0
2	67.8	37.9	36	43.2	41	458.4	0.7	5	99.1580729	379
3	75.2	0.0	0	93.7	89					
4	75.1	3.2	3	93.7	89	637.2	0.4	2	99.47916667	382
5	52.7	17.9	17	80.0	76	670.6	0.7	3	99.05442708	380
6	109.0	0.5	1	98.8	92	611.6	1.2	6	98.7223958	378
7	83.6	1.1	1	97.9	93					
8	64.6	10.5	60	77.0	3	473.9	1.1	7	98.74505208	374
9	111.1	3.3	7	90.1	72	880.6	0.5	3	99.37604167	381
10	62.4	11.6	11	88.4	84	497.9	1.5	5	97.62005208	379
11	77.0	0.8	1	93.5	87	798.8	0.8	5	99.1302083	379
12	86.0	0.7	1	90.7	76					
13	65.3	0.0	0	86.3	82					
14	47.3	3.2	3	64.2	61	53.1	6.5	53	70.33203125	217
15	73.3	0.0	0	94.9	89	553.9	9.8	119	82.3257812	177
16	75.3	4.2	4	71.6	68					
17	59.2	7.8	16	72.9	39	625.9	0.8	4	98.94192708	378
18	53.6	1.1	1	91.6	87	711.4	1.1	6	98.8440104	378
19	41.3	20.0	19	71.4	66					
20	93.4	0.0	0	100.0	95	270.1	4.1	54	94.625	313
21	40.6	7.4	7	51.9	49					
22	66.9	2.1	2	93.7	89	0.6	99.7	384	0	0
23	53.6	0.0	0	84.9	80	379.7	0.4	2	99.47916667	382

24	71.6	0.0	0	64.2	61	568.6	0.4	2	99.47916667	382
25	68.5	0.0	0	92.9	87	165.5	1.3	5	97.76302083	374
26	46.9	5.3	5	65.3	62	263.1	1.3	5	98.69791667	379
27	30.5	12.6	12	32.8	31	74.0	1.8	7	93.37760417	349
28	55.2	0.0	0	82.1	78	709.7	0.6	2	98.75260417	382
29	76.4	0.0	0	93.7	89					
30	90.0	1.1	1	95.8	91	518.0	1.1	7	98.5570313	373
31	93.5	1.0	2	81.2	55					
32	72.2	0.0	0	92.6	88					
33	80.8	1.4	3	79.4	52	559.5	0.6	3	99.32447917	380
34	62.8	0.0	0	93.7	89	475.3	0.4	2	99.20208333	381
35	75.4	0.0	0	94.7	90	675.6	0.3	2	99.47916667	382
36	59.1	0.0	0	93.4	88	353.3	1.0	4	98.95833333	380
37	36.4	3.1	4	44.3	35	0.7	99.3	383	0.312760417	0
38	74.1	7.9	49	80.8	24	316.4	0.7	4	99.20859375	379

Table S3. Coverage statistics for both amplicon panels.

For the PCRs / GSJunior panel (n=96), PCRs were performed using specific primers (available upon request), with Fast Start High Fidelity Taq (Roche Life Science) following the manufacturer's protocol. Sequencing was performed with the Roche GS Junior 454 sequencing system, following the manufacturer's protocol.

For the Fluidigm / MiSeq panel (n=384), PCRs were performed using specific primers (Fluidigm D3 Assay Design), with Fast Start High Fidelity Taq (Roche Life Science), using the Fluidigm Access Array, following the manufacturer's protocol. Sequencing was performed with the MiSeq sequencing system (2x300bp, V5), following the manufacturer's protocol.

Supplemental Table S4

Comment	Chromosome	Position	Reference	Alternative	Aminoacid change	SIFT score	Polyphen2_HDIV score	Polyphen2_HVAR score	MutationTaster score	GERP ++	PhyloP 46 way	EVS chromosome count	ExAC chromosome count
	10	95381695	A	G	NM_006204.2:c.730A>G:p.Met244Val	0 (D)	0.046 (B)	0.023 (B)	0.846 (D)	3.64	2.166	G=1/A=13005	G=1/A=121365
	10	95386461	C	T	NM_006204.2:c.1004C>T:p.Pro335Leu	0.02 (D)	0.996 (D)	0.732 (P)	1 (D)	4.58	2.89	T=0	T=8/C=118458
Causative *FA2H* homozygous variant validated in the family	10	95399849	G	A	NM_006204.2:c.1505G>A:p.Arg502His	0.08 (T)	0.76 (P)	0.136 (B)	1 (N)	-2.12	-0.561	A=0	A=4/G=121342

Table S4. Characteristics of other *PDE6C* variants found by panel sequencing.

Summary of characteristics for all *PDE6C* variants found by panel sequencing in 384 individuals. Annotation was performed using Annovar (www.openbioinformatics.org/annovar/).[2] The database frequencies originate from 1000 genomes (www.1000genomes.org/), Exome Variant Server (EVS, http://evs.gs.washington.edu/EVS) and Exome Aggregation Consortium (ExAC, http://exac.broadinstitute.org/). Pathogenicity scores are evaluated as follows: SIFT (http://sift.jcvi.org/) predicts deleteriousness (D) under 0.05; the variant was else considered tolerated (T); Polyphen2 (http://genetics.bwh.harvard.edu/pph2/) classifies SNPs as probably damaging (D; HDIV>=0.957, HVAR>=0.909), possibly damaging (P; 0.453<=HDIV<=0.956, 0.447<=pp2_hdiv<=0.908), or benign (B; HDIV<=0.452, HVAR <=0.446); MutationTaster (http://www.mutationtaster.org/) classifies them as "disease_causing_automatic" (A), "disease_causing" (D), "polymorphism" (N) or "polymorphism_automatic" (P) with a given probability value, 1 being the most probable. For both GERP++ (http://mendel.stanford.edu/SidowLab/downloads/gerp/) and PhyloP (http://compgen.bscb.cornell.edu/phast/help-pages/phyloP.txt), higher scores indicate better residue conservation.

Supplemental Table S5

Individual	Chr	Position	Ref	Alt	Amino acid change	Variant(s) in other genes involved in ADCA	Sanger confirmation	Segregation within family	Electrophysiological evidences	SIFT score	Polyphen2_HDIV score	Polyphen2_HVAR score	MutationTaster score	GERP++	phyloP 46way	Maximal Population Frequency	1000G ALL	ExAC ALL	EVS ALL
Pathogenic variant (3 Strong PS1 according to ACMG guidelines, Richard et al., 2015)																			
recurrent : AAD-SAL-233, AAD-GRE-319, AAD-SAL-454	17	48694921	G	A	NM_018896:c.5144G>A:pArg1715His	No	Yes	6 affected in AAD-SAL-233, 3 affected in AAD-GRE-319	statistically significant alterations of activation and inactivation curves	0 (D)	1 (D)	1 (D)	D (1)	5.02	2.348	.	.	.	.
Variants of Unknown Significance (VUS)																			
H202	17	48674228	C	T	NM_018896:c.3202C>T:p.Arg1068Cys	NA	Yes	NA	no statistically significant difference	0.03 (D)	1 (D)	0.999 (D)	D (1)	2.78	1.052	0.0002	.	0	.
H202	17	48703688	C	A	NM_018896:c.6710C>A:p.Pro2237His	NA	Yes	NA	no statistically significant difference	0.02 (D)	0.994 (D)	0.974 (D)	N (1)	4.32	2.484	0.0023	0.0002	0.0005	0.0003
K087	17	48692795	C	A	NM_018896:c.4833C>A:p.His1611Gln	NA	Yes	NA	no statistically significant difference	0.79 (T)	0.999 (D)	0.993 (D)	D (1)	4.75	2.17	.	.	.	.
7909	17	48677170	C	A	NM_018896:c.3640C>A:p.Pro1214Thr	NA	Yes	NA	NT	0.4 (T)	0.042 (B)	0.07 (B)	N (1)	0.264	-0.055	.	.	.	.
SAL-REB-399-400	17	48701820	C	T	NM_018896:c.6329C>T:p.Thr2110Ile	NA	Yes	NA	NT	0.22 (T)	0.43 (B)	0.24 (B)	N (1)	2.88	1.338	.	.	.	.
AAD-BOR-SAR-565-012	17	48678124	G	A	NM_018896:c.3728G>A:p.Arg1243Gln	NA	Yes	NA	NT	0.06 (T)	0.999 (D)	0.98 (D)	N (1)	5.46	2.569	0.005	0.001	0.0001	.
AAD-SAL-MAR-931-001	17	48650036	G	T	NM_018896:c.868G>T:p.Gly290Trp	No	Yes	NA	NT	0.02 (D)	1 (D)	1 (D)	D (1)	5.36	2.541	.	.	.	.
AAD-LIL-SEP-246-001	17	48673978	G	A	NM_018896:c.3035G>A:p.Gly1012Asp	No	Yes	NA	NT	0.48 (T)	1 (D)	0.999 (D)	D (0.869)	4.14	2.375	0.0003	.	0.0001	0.0002
AAD-STR-ALB-916-001	17	48703471	C	T	NM_018896:c.6493C>T:p.Arg2165Trp	Missense monoallelic VUS in *POLG*	Yes	NA	NT	0.02 (D)	1 (D)	0.958 (D)	N (0.996)	4.3	1.217	0	.	0	.
AAD-GRE-CUI-568-014	17	48649991	C	T	NM_018896:c.823C>T:p.Arg275Cys	Missense VUS in *REEP1*	Yes	Present in unaffected mother	NT	0.01 (D)	1 (D)	0.999 (D)	N (0.99)	4.37	1.234	0.0004	.	0.0001	.
Variants of Unknown Significance AND pathogenic variant in another gene involved in ADCA																			
AAD-BOR-BAR-414-003	17	48685335	C	T	NM_018896:c.4660C>T:p.Arg1554Trp	Frameshift in *CACNA1A* (to confirm)	Yes	NA	NT	0.01 (D)	1 (D)	0.997 (D)	D (1)	3.71	2.196	0.0001	.	0	.
AAD-SAL-JAC-070-007	17	48674121	G	A	NM_018896:c.3095G>A:p.Arg1032Gln	Frameshift in *CACNA1A*, missense monoallelic VUS in *POLG* (to confirm)	Yes	NA	NT	0.27 (T)	0.88 (P)	0.329 (B)	N (0.867)	0.624	-0.086	.	.	.	.

Table S5. Characteristics of other *CACNA1G* variants found by panel sequencing.

Summary of characteristics and pathogenicity evidences for all *CACNA1G* variants encompassed by panel sequencing. All scores are described in Table S2. No other variant than p.Arg1715His could lead to a definite conclusion regarding its pathogenicity, due to lack of other affected for segregation confirmation, or lack of functional proof. Only one other variant, p.Gly290Trp, is predicted pathogenic by all *in silico* softwares and is never present in public databases. No variant is located nearby p.Arg1715His, nor in S4 segments, regardless of the domain. All variants were therefore classified as variant of unknown significance (VUS).[4]

Chr: Chromosome
NA: not available
NT: not tested
Ref / Alt: reference and alternative base
VUS: variant of unknown significance (ACMG class 3)

Supplemental Table S6

	WT		His1611Gln		Arg1068Cys		Pro2273His	
	Mean±SEM	n	Mean±SEM	n	Mean±SEM	n	Mean±SEM	n
Current density (pA/pF)	-74.58±11.18	19	-43.47±13.35	4	-92.3±22.12	9	-68.76±16.79	6
$V_{1/2}$ act (mV)	-47.2±0.65	18	-45.61±0.27	4	-47.01±0.63	8	-44.89±0.88	6
K $_{Vact}$ (mV)	4.761±0.14	18	5.08±0.17	4	4.87±0.26	8	4.911±0.19	6
$V_{1/2}$inact (mV)	-70.91±0.48	15	-70.07±0.39	4	-72.61±1.19	9	-69.54±0.46	6
K $_{Vinac}$ (mV)	4.29±0.07	15	3.96±0.03	4	4.50±0.19	9	4.7±0.22	6
τ_{act} at -40 mV (ms)	4.38±0.39	10	4.15±0.28	4	3.59±0.19	4	3.94±0.28	5
τ_{inact} at -40 mV (ms)	16.27±0.77	10	17.03±1.59	4	13.8±0.96	4	15.45±0.53	5
recovery (ms)	105.1±9.48	12	103.5±7.08	4	81.45±3.18	4	91.69±3.41	5
τ_{deact} at -70mv (ms)	3.87±0.25	8	3.65±0.33	3	3.18±0.148	4	3.44±0.29	6

Table S6. Electrophysiological properties of additional Cav3.1 variants.

V1/2 represents the half-activation and respectively half inactivation potential, K the slope factor, τact τinact and τdeact the activation, inactivation and respectively deactivation kinetics. n is the number of cells. No statistically significant differences were seen between the WT and the different variants presented in this table.

Supplemental References

1 Abecasis, G.R., Cherny, S.S., Cookson, W.O., Cardon, L.R. (2002). Merlin-rapid analysis of dense genetic maps using sparse gene flow trees. Nat. Genet. *1*, 97-101.

2 Wang, K., Li, M., Hakonarson, H. (2010). ANNOVAR: Functional annotation of genetic variants from next-generation sequencing data. Nucleic Acids Research. *38*, e164.

3 Chun, S., Fay, J.C. (2009). Identification of deleterious mutations within three human genomes. Genome Res. *19*:1553-1561.

4 Richards, S., Aziz, N., Bale, S., Bick, D., Das, S., Gastier-Foster, J., Grody, W., Hegde, M., Lyon, E., Spector, E., et al., on behalf of the ACMG Laboratory Quality Assurance Committee (2015). Standards and guidelines for the interpretation of sequence variants: a joint consensus recommendation of the American College of Medical Genetics and Genomics and the Association for Molecular Pathology. Genet. Med. *17*, 405-423.